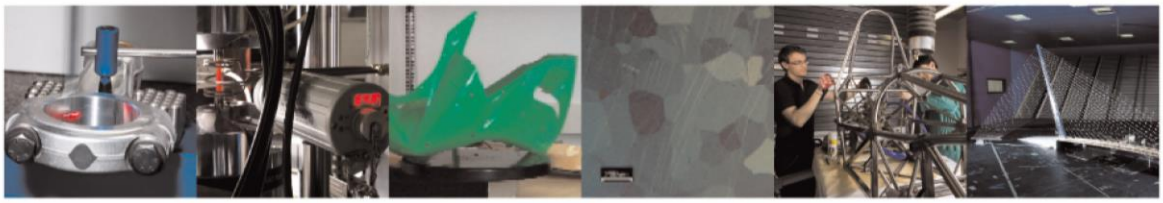

Upgraded stability analysis of milling operations by means of advanced modeling of tooling system bending

Totis, G; Albertelli, P.; Torta, M.; Sortino, M.; Monno, M.

This is a post-peer-review, pre-copyedit version of an article published in INTERNATIONAL JOURNAL OF MACHINE TOOLS & MANUFACTURE. The final authenticated version is available online at: http://dx.doi.org/10.1016/j.ijmachtools.2016.11.005

DIPARTIMENTO DI MECCANICA ■ POLITECNICO DI MILANO
via G. La Masa, 1 ■ 20156 Milano ■ EMAIL (PEC): pecmecc@cert.polimi.it
http://www.mecc.polimi.it
Rev. 0

Upgraded stability analysis of milling operations by means of advanced modeling of tooling system bending

Abstract

The problem of undesired self-excited chatter vibrations in milling is very common. However, only in the last two decades some significant achievements for the theoretical understanding of this intricate phenomenon have been accomplished. Nevertheless, state of the art dynamic models are still not able to completely explain milling dynamics and chatter onset during some conventional milling operations performed by conventional cutting tools. In this research work, a revolutionary model of tooling system dynamics and of the regenerative effect in milling will be presented. The new model introduces a significant correction to the predicted stability borders when the cutter diameter is relatively large in comparison with tooling system overhang and when curved or inclined cutting edges are applied. Accordingly, the new approach may be of great interest for many industrial applications. The model has been successfully validated by performing experimental modal analysis, cutting force coefficient identification and stability lobes diagram determination, through many specific cutting tests. In the considered case study, where the afore mentioned geometrical features of the tooling system were still moderate, a significant shift of the stability borders of about +25% was experimentally observed and correctly predicted by the new approach.

Keywords: Milling, Dynamics, Modeling, Chatter, Prediction

Preprint submitted to International Journal of Machine Tools and Manufacture, November 10, 2016

1. Introduction

When performing machining operations in manufacturing industry, undesired vibrations of the machining system may frequently arise, which do strongly affect dimensional accuracy and surface quality of the machined parts, thus hindering the achievement of the required part specifications.

Basically, machining vibrations can be classified as free vibrations, forced vibrations and self-excited chatter vibrations.

Free vibrations are caused by time-varying, aperiodic cutting conditions: they tend to extinguish rapidly and their effects on the process are usually negligible.

Forced vibrations are due to time-varying periodic cutting forces: they can be easily attenuated by selecting adequate spindle speeds, in order to avoid triggering the mechanical resonances of the machining system.

On the contrary, self-excited chatter vibrations are due to other complex physical phenomena and they cause bad surface quality and dimensional inaccuracies of the machined parts [1][2][3], thus implying productivity losses and many other problems. For instance, they may greatly increase tool wear rate [4] and they may damage machine tool components. For these reasons, chatter vibrations should be absolutely avoided.

Self-excited regenerative chatter vibrations were first observed by Taylor at the beginning of the 20^{th} century. In the sixties, Tobias [5] was one of the first authors that started dealing with the theory governing chatter vibrations. In the same period, Merritt [6] proposed a block diagram, inspired by the theory of feedback control, for representing the regenerative effect in metal cutting. At the end of the seventies at CIRP, Tlusty [7] presented a preliminary study on the effects of the dynamic properties of the system on chatter vibrations in turning. Smith and Tlusty [8] proposed an efficient programming approach for chatter simulation. All the early research works refer to quite simplified case studies (i.e. turning operations with simple dynamics). Only in the ninetiees Altintas and Budak [9] proposed a first, still rough but very illuminating model of regenerative chatter vibrations in milling.

However, since the second half of nineteenth century several strategies have been developed for solving this challenging problem.

Simple passive approaches are mostly adopted, aiming at avoiding the phenomenon by including special mechanical components into the machining system, such as tool adapters with high stiffness and damping properties [10],

cutters with uneven teeth spacing [11] and other devices [12]. For instance, materials with high damping properties can be used in machine tools [13] and sub-components design [14].

Alternatively, semi-active chatter suppression strategies are emerging, aiming at disturbing chatter onset by continuously modulating the modal parameters of the tooling system [15][16] or some fundamental kinematic parameters such as the spindle speed, as in the Spindle Speed Variation technique [17].

Active techniques can be also applied, aiming at reducing tooling system vibrations [18] or workpiece vibrations [19] by using feedback control loops involving sensors and actuators. Nevertheless, such techniques are rarely proposed in literature and not widespread at commercial-industrial level due to their high complexity and cost [20].

Other effective strategies are based on sensor-based chatter onset detection by adequate monitoring systems installed into the machine tools, combined with algorithms for automatic selection of optimal cutting parameters [21]. A similar approach has already been applied on high-end commercial machine tools [22], where a preliminary empirical evaluation of process stability with different spindle speed levels can be carried out before starting the production job; by so doing, an optimal spindle speed can be automatically selected.

Last but not least, the predictive strategies consist in the application of numerical algorithms for the preventive evaluation of process stability with different combinations of cutting parameters. By so doing, the so called stability lobes can be obtained, which may be useful for the selection of optimal stable cutting conditions [23][24][25].

A deep theoretical understanding and accurate modeling of the physical mechanisms causing chatter vibrations are crucial for a successful implementation of the afore mentioned methodologies.

In milling, the main physical phenomena influencing chatter onset are:

- the regenerative effect, which is the influence of the undulation left on the workpiece by the previous tooth passage on the actual uncut chip thickness acting on the tooth passing through the same angular position [26][1][2];

- process damping, which derives from the interference between the machined surface and tool clearance [27][28];

- mode coupling, deriving from the dynamic cross interactions between different directions in the working plane orthogonal to spindle axis [29][30][31][32];
- chaotic dynamics arising from cutting process non-linearities [33][34], effective stress distribution on the normal rake face [1], thermoplastic behaviour of the chip material [35] or other less common mechanisms.

Chatter mechanisms are usually classified as primary or secondary. In the low spindle speed range chatter onset is mostly influenced by the so called primary chatter mechanisms [36][7], such as process damping and the other physical phenomena related to the friction between tool and chip/workpiece on contact surfaces. On the contrary, in the medium-high spindle speed range secondary chatter - i.e. the regenerative effect - is dominant.

The first significant attempt for analytical modeling of regenerative chatter vibrations in milling was proposed by Altintas and Budak in 1995 [9]. Since then, some great advances have been carried out, as will be illustrated in next section. Still, there are some open issues to be solved, such as those addressed in this work.

According to most current models, the instantaneous chip thickness evaluation on a given cutting tooth is performed by only considering tool tip transversal vibrations in the working plane orthogonal to spindle axis. Moreover, only the transverse forces are taken into account for modeling tooling system deflection, while the momenta deriving from axial forces are neglected.

This is a sufficient approximation when considering slender tooling systems - such as cylindrical end-mills or some bull-nose cutters - with a small diameter D in comparison to the total tool overhang L, or when the working cutting edge is approximately straight and parallel to spindle axis (average working cutting edge angle $\chi \approx 90°$).

Nevertheless, when considering tooling systems with a relatively large D/L ratio, which show at the same time an inclined cutting edge (average working cutting edge angle $\chi < 90°$), this approximation may strongly affect the accuracy of the predicted stability borders.

In this paper, a revolutionary model of milling dynamics will be introduced for improving prediction accuracy in the afore mentioned cases.

The proposed model represents a generalization of the state of the art model, which is recovered in the limit $D/L \ll 1$ or $\chi \approx 90°$.

The paper is structured as follows. Firstly, the state of the art about regenerative chatter modeling in milling will be illustrated. In the following

section, an enhanced model of milling dynamics will be proposed, together with an advanced and compact cutting force model. Afterwards, a brand new cutter-workpiece interaction model will be presented. Then, the criteria for stability evaluation will be illustrated. Finally, the new model will be experimentally validated by performing modal analysis, cutting force coefficients identification and stability lobes diagram determination through several specific cutting tests.

2. Literature review on regenerative chatter modeling in milling

The overall dynamic compliance of the machining system is dominated by the most flexible element of the kinematic chain, which is usually the spindle - tooling system [37]. Sometimes, vibration eigenmodes of the whole machine tool structure may play a significant role, especially for workpiece materials requiring low cutting speeds. Besides, in the presence of very thin workpiece structures - such as turbine blades - workpiece dynamics cannot be neglected too, as shown in [38] and [39].

However, only transverse vibrations between tool and workpiece in the working plane orthogonal to spindle axis are generally considered for the estimation of the current chip thickness, depending on the actual and delayed cutter vibrations. The effects of other degrees of freedom are usually supposed negligible throughout literature. One very recent exception is the work of Kilic et al. [40] presenting a generalized model for cutting mechanics and dynamics which theoretically includes all possible translational and rotational degrees of freedom (6 in total) for accurately modeling regenerative chip thickness in generic conditions. However, the consequence of this idea in conventional face milling with large diameter cutters was neither investigated nor implemented or validated.

The most simple dynamic milling model involves a single oscillating direction described by a single harmonic oscillator, as assumed in [41] and [42]. Nevertheless, the validity of this model is limited to very few industrial cases. A typical milling process requires at least two degrees of freedom, each approximated by a single harmonic oscillator [43][23]. In many practical cases several harmonic oscillators have to be even included along each direction, in order to model machining system dynamics with sufficient accuracy [25][44][45][27].

Cutting forces tend to amplify regenerative vibrations, thus a correct modeling of cutting forces is crucial. In particular, cutting force variations

due to regenerative perturbations have to be accurately estimated. Several approaches have been proposed in literature in the last decades, which can be roughly classified in two categories. The mechanistic-empirical models are based on several cutting force coefficients that are determined by linear regression on measured cutting forces [37]. Nevertheless, they are sometimes lacking of physical insight. On the other side, the oblique cutting models can be very sophisticated and well physical-grounded [46], though not very easy to apply in practice. Some recent works are an intelligent combination of the two approaches, combining the effectiveness of the mechanistic approach with the physical depth of the oblique cutting theory [40][47][48].

Process kinematics have a great impact on milling dynamics too. For instance, the stability borders are influenced by milling configuration (up or down milling [42]), by the radial immersion between tool and workpiece a_L/D [43] and by other kinematic parameters.

Last but not least, the regenerative effect is influenced by the geometrical details of the cutter, as illustrated in [49][45][50][51], which affect the dynamic interaction between tool and workpiece.

Nevertheless, there is still an incomplete understanding of some important phenomena affecting the regenerative effect.

Specifically, according to current models the instantaneous chip thickness perceived by a single cutting flute does only depend on the transversal vibrations u_x and u_y of cutter tip barycentre in the working plane. Similarly, only the transverse forces F_x and F_y are taken into account for modeling tooling system deflection, while the momenta M_x and M_y deriving from axial forces are in general neglected.

As stated in the introduction, this is a sufficient approximation when considering slender tooling systems with a small D/L ratio, as the cylindrical endmills extensively studied in literature [43][23][49][51].

Nevertheless, when considering tooling systems with a relatively large D/L ratio (for instance $D/L > 1/3$) and with curved or inclined cutting edges, as in the following cases

- general face milling cutters with $\chi_1 = 45°$,
- face shoulder cutters with $\chi_1 = 90°$ and with large nose radius r_ε,
- round insert cutters for face milling and profiling,
- bull-nose endmills and many other special geometries

the classical model based on transversal vibrations and forces alone is not adequate anymore.

It is indeed a well known empirical truth among technicians working in the shop-floor that an average $\chi < 90°$ tends to stabilize the process in comparison to the case $\chi \approx 90°$, especially for large diameter cutters. This is due to a presumed stabilizing effect of the axial forces and to other unclear physical phenomena. Nevertheless, no mathematical/numerical demonstration of this fact has ever been available in literature.

In this paper, this theoretical gap will be covered thanks to the proposed generalization of the classical model which will now include

- the rotational degrees of freedom ϑ_x and ϑ_y describing tool tip rotation in the ZY and ZX coordinate planes containing spindle axis;
- the momenta M_x and M_y associated to the axial forces acting on cutter teeth.

By so doing, the accuracy of the predicted stability borders will be significantly improved, especially for the afore mentioned tooling system geometries.

In the following sections, the details of the new model will be illustrated.

3. New model of milling dynamics

In milling, the spindle-toolholder-cutter system is classically represented by a Jeffcott rotor [52] rotating at constant speed n around its main axis and vibrating along the two directions orthogonal to cutter axis of an inertial, non rotating coordinate frame $OXYZ$, as illustrated in Figure 1.

The system is considered rigid in the pure axial and torsional directions. For the sake of simplicity, the workpiece is also considered to be rigid.

According to the state of the art approach, only the transverse vibrations and forces are considered in the global dynamic model, as follows

$$\begin{bmatrix} u_x \\ u_y \end{bmatrix} = \begin{bmatrix} W_{uxFx} & W_{uxFy} \\ W_{uyFx} & W_{uyFy} \end{bmatrix} \begin{bmatrix} F_x \\ F_y \end{bmatrix} \approx \begin{bmatrix} W_{uxFx} & 0 \\ 0 & W_{uyFy} \end{bmatrix} \begin{bmatrix} F_x \\ F_y \end{bmatrix} \quad (1)$$

where the cross transfer functions W_{uxFy} and W_{uyFx} are usually negligible. Accordingly, only the direct transfer functions W_{uxFx} and W_{uyFy} are generally considered for describing tooling system dynamics.

These transfer functions are typically obtained by performing modal analysis on the tooling system in steady conditions, i.e. when the spindle is not rotating. When spindle is rotating, it tends to oscillate along X and Y directions according to the same transfer functions, as if spindle dynamics were unaffected by spindle rotation. This assumption is practically adopted by all state of the art models, and its validity was experimentally confirmed by many authors in the last two decades. Of course, some deviations from this behavior could occur due to gyroscopic effects or other minor effects arising at high spindle speeds. In this work, this assumption will be also implicitly adopted for the new model. It will be of further interest to investigate the deviation of the effective dynamic behavior from that measured in steady conditions when spindle speed is increased in future works.

In order to improve the above dynamic model, tool tip rotations ϑ_x and ϑ_y in the YZ and XZ coordinate planes as well as the bending momenta M_x and M_y should be introduced. This implies the following generalization

$$\begin{bmatrix} u_x \\ \vartheta_y \\ u_y \\ \vartheta_x \end{bmatrix} = \begin{bmatrix} W_{uxFx} & W_{uxMy} & W_{uxFy} & W_{uxMx} \\ W_{\vartheta yFx} & W_{\vartheta yMy} & W_{\vartheta yFy} & W_{\vartheta yMx} \\ W_{uyFx} & W_{uyMy} & W_{uyFy} & W_{uyMx} \\ W_{\vartheta xFx} & W_{\vartheta xMy} & W_{\vartheta xFy} & W_{\vartheta xMx} \end{bmatrix} \begin{bmatrix} F_x \\ M_y \\ F_y \\ M_x \end{bmatrix} \tag{2}$$

where all the quantities are functions of the imaginary pulsation $j\omega$. The bending momenta M_x and M_y will arise from the axial forces acting on cutter teeth, which may be significant when the average working cutting edge angle χ is relatively small, as will be described in the next sections.

Each transfer function can be expressed as a sum of harmonic oscillators, i.e.

$$W(j\omega) = \sum_{k=1}^{M} \frac{G_k}{(j\omega/\omega_{n,k})^2 + 2\xi_k (j\omega/\omega_{n,k}) + 1} \tag{3}$$

where G_k is the zero frequency gain or static compliance, $\omega_{n,k}$ is the natural pulsation and ξ_k is the damping coefficient of the k_{th} mode of vibration. In general, the modal parameters may change from one transfer function to the other. However, some assumptions will be adopted for model optimization, as will be explained in the following.

3.1. Toy model based on Euler-Bernoulli beam element

Let us consider a Finite Element beam with circular cross section based on Euler-Bernoulli model, in cantilever configuration, approximating the tooling

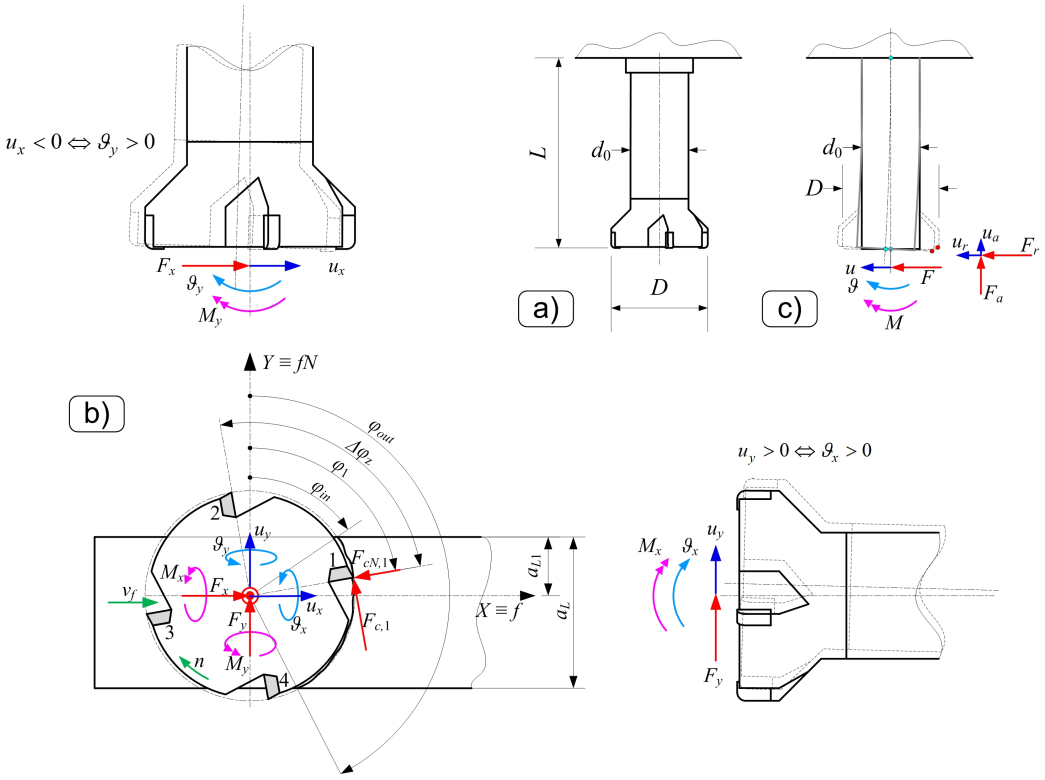

Figure 1: Reference scheme for relative tool-workpiece vibrations

system. Let us consider the average toolholder diameter d_0 as the beam external diameter, which may be smaller or equal to the cutter external diameter D. Eventually, let us assume the total tooling system overhang L as the total beam length, as illustrated in Figure 1 (a) and (c).

Let E be the Young modulus and J be the moment of inertia given by

$$J = \frac{\pi d_0^4}{64} \tag{4}$$

Let u and ϑ be the radial displacement and rotation of beam free tip, where the radial force F and momentum M can be applied. From the Euler-Bernoulli theory one can easily derive the following static compliance relations

$$\begin{cases} u = \frac{L^3}{3EJ}F + \frac{L^2}{2EJ}M = H_{uF}F + H_{uM}M \\ \vartheta = \frac{L^2}{2EJ}F + \frac{L}{EJ}M = H_{\vartheta F}F + H_{\vartheta M}M \end{cases} \tag{5}$$

It is worth noting that all static compliance can be expressed as proportional to the displacement-force flexibility, as follows

$$\begin{cases} H_{uM} = \nu H_{uF} \\ H_{\vartheta F} = \nu H_{uF} \\ H_{\vartheta M} = \mu H_{uF} \end{cases} \tag{6}$$

where

$$\nu = \frac{3}{2L}; \qquad \mu = \frac{3}{L^2} \tag{7}$$

If we consider the dynamic Euler-Bernoulli beam element including inertial and damping matrixes, we will finally obtain the dynamic version of Equation (5). Specifically, one obtains

$$\begin{cases} u(j\omega) = W_{uF}(j\omega) F(j\omega) + W_{uM}(j\omega) M(j\omega) \\ \vartheta(j\omega) = W_{\vartheta F}(j\omega) F(j\omega) + W_{\vartheta M}(j\omega) M(j\omega) \end{cases} \tag{8}$$

It can be easily shown that each transfer function of this basic model encloses two resonances. Since the first, low-frequency resonance is dominant in our case, it will be sufficient to focus on that in order to get a realistic representation of system dynamics. Under this assumption, the following simplification can be carried out

$$\begin{cases} W_{uM}(j\omega) \approx \nu W_{uF}(j\omega) \\ W_{\vartheta F}(j\omega) \approx \nu W_{uF}(j\omega) \\ W_{\vartheta M}(j\omega) \approx \mu W_{uF}(j\omega) \end{cases} \tag{9}$$

In other words, the dynamic transfer functions are approximately proportional to the displacement-force transfer function, by means of the same constants evidenced in static conditions as shown by the example of Figure 2.

This can be further clarified by recalling that the first eigenmode of a cantilever beam configuration is the dominant term of the transfer function from the static gain to the corresponding resonance peak. Thus, static relations between forces, moments, displacement and rotations of tooling system free end are practically preserved up to the first resonance peak, where tooling

system shape does practically coincide to the first eigenmode, whose oscillations around the rest configurations are simply amplified when the excitation frequency is close to the resonance peak.

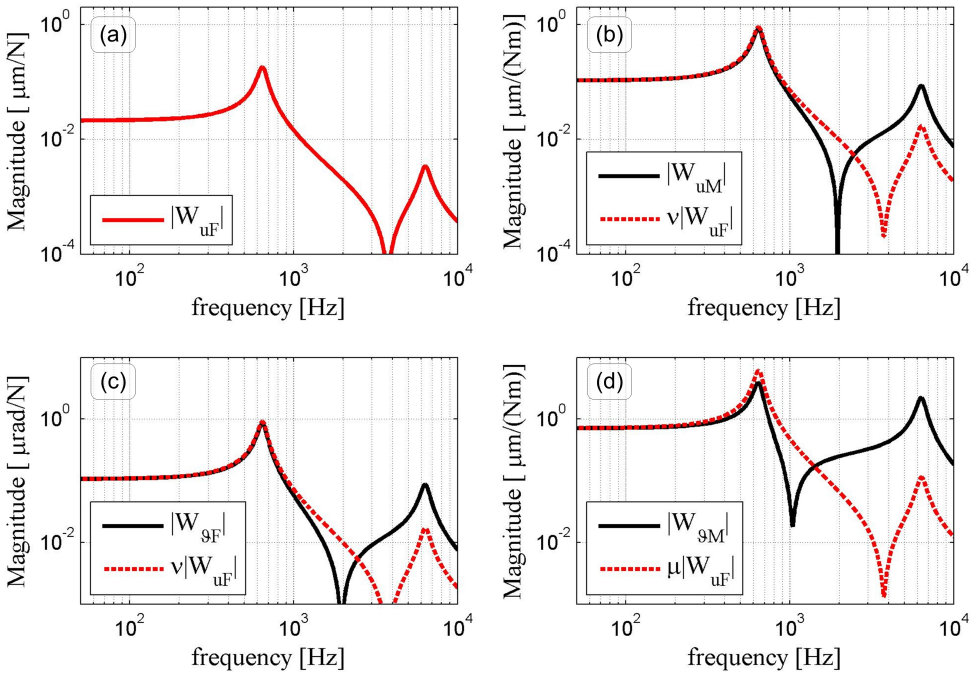

Figure 2: Example of transfer functions for describing tooling system bending in a given plane, when considering a tooling system made of conventional steel (Young modulus $E = 210$ GPa, density $\rho = 7.81$ g/cm^2) with average diameter $d_0 = 80$ mm and total overhang $L = 300$ mm. (a) Main, classical transfer function connecting transverse vibration u to transverse force F. (b) Transfer function connecting transverse vibration u to bending moment M. (c) Transfer function connecting tooling system rotation ϑ to transverse force F. (d) Transfer function connecting tooling system rotation ϑ to bending moment M.

In most cases the effect of M on ϑ through $W_{\vartheta M}$ is negligible, since μ or M are small. As a consequence, the following important relation holds

$$\vartheta\left(j\omega\right) \approx \nu u\left(j\omega\right) \tag{10}$$

Another important topic is the determination of the radial displacement u_r

as well as the axial displacement u_a of the cutter tooth located at the right at $D/2$ from tooling system axis. According to signs conventions adopted in Figure 1, they are given by

$$\begin{cases} u_r(j\omega) = u(j\omega) \\ u_a(j\omega) = -\frac{D}{2}\vartheta(j\omega) \end{cases} \tag{11}$$

Moreover, let us suppose that the equivalent nodal forces depend on the radial F_r and axial F_a forces shown in Figure 1, which are applied at $D/2$ from beam axis. Thus

$$\begin{cases} F(j\omega) = F_r(j\omega) \\ M(j\omega) = -\frac{D}{2}F_a(j\omega) \end{cases} \tag{12}$$

where it should be recalled that in general $D \neq d_0$, since D is the external cutter diameter while d_0 is the toolholder average diameter.

Therefore, after some algebraic manipulations one may obtain

$$\begin{cases} u_r(j\omega) \approx W_{uF}(j\omega)\left[F_r(j\omega) - \eta F_a(j\omega)\right] \\ u_a(j\omega) \approx W_{uF}(j\omega)\left[-\eta F_r(j\omega) + \lambda F_a(j\omega)\right] \end{cases} \tag{13}$$

where

$$\eta = \frac{3}{4}\frac{D}{L}, \qquad \lambda = \frac{3}{4}\left(\frac{D}{L}\right)^2 \tag{14}$$

are aspect ratio factors which will be very important in the following. If we assume a realistic aspect ratio of about

$$\frac{D}{L} \approx \frac{1}{3} \Rightarrow \eta \approx 25\%, \quad \lambda \approx 8\% \tag{15}$$

Under this hypothesis, the influence of the axial force on the transverse displacement cannot be ignored. Specifically, it partially compensates the destabilizing effect of the radial force.

Under the above hypothesis, it should be also noticed that the size of the axial displacement cannot be neglected in comparison with the radial displacement. However, the axial displacement is mainly due to the radial force, while its dependence on the the axial force - i.e. on bending momentum - can be neglected.

3.2. Cutter dynamics during rotation

Let us now model the effective dynamics of the cutter during rotation. First of all, the transverse vibrations u_x ad u_y are now given by

$$\begin{cases} u_{x,j}(j\omega) = u_x(j\omega) = W_{uxFx}(j\omega) F_x(j\omega) - W_{uxMy}(j\omega) M_y(j\omega) \\ u_{y,j}(j\omega) = u_y(j\omega) = W_{uyFy}(j\omega) F_y(j\omega) + W_{uyMx}(j\omega) M_x(j\omega) \end{cases} \tag{16}$$

where the displacement-momentum transfer functions are assumed proportional to the direct transfer functions W_{uxFx} and W_{uyFy}, as follows

$$\begin{cases} W_{uxMy}(j\omega) \approx \nu_y W_{uxFx}(j\omega) \\ W_{uyMx}(j\omega) \approx \nu_x W_{uyFy}(j\omega) \end{cases} \tag{17}$$

In accordance with the Euler-Bernoulli toy model of previous subsection (Equation (10)), the cutter body small rotations ϑ_x and ϑ_y in the ZY and ZX cartesian planes are assumed proportional to the transverse vibrations u_x and u_y - by means of the same proportionality constants ν_y and ν_x - i.e.

$$\begin{cases} \vartheta_y(j\omega) \approx -\nu_y u_x(j\omega) \\ \vartheta_x(j\omega) \approx \nu_x u_y(j\omega) \end{cases} \tag{18}$$

Moreoever, this result is expected from the previous considerations on the Euler-Bernoulli model

$$\nu_y \cong \nu_x \cong \frac{3}{2L} \tag{19}$$

Finally, the axial vibrations of the j-th tooth can be computed in the time domain using the following relation

$$u_{z,j}(t) = R\cos(\varphi_j(t))\,\vartheta_x(t) - R\sin(\varphi_j(t))\,\vartheta_y(t) \tag{20}$$

where φ_j is the feed motion angle of the j-th tooth and R is the local radius where the considered cutting edge point is located. For face milling cutters with cemented carbide inserts this radius is approximately constant along the whole cutting edge, and it is $R \cong \frac{D}{2}$, where D is the external cutter diameter.

It is worth noting that the new model is 3D while the classical model is 2D, since the axial vibrations $u_{z,j}$ of each tooth are now considered in addition to transverse vibrations u_x and u_y.

3.3. Cutting force model

Cutting forces depend on several factors, such as workpiece material, cutting parameters, cutter geometry and milling process geometry. Let us consider a milling operation performed with a constant pitch milling cutter with Z_t cutting inserts or flutes, nominal working cutting edge angle χ_1, nose radius r_ε.

Let us suppose constant speed machining conditions, i.e. no modulation of spindle speed is applied. Let Ω be the angular spindle speed expressed in rad/s, while n is the spindle speed in rpm. Thus we have

$$\Omega = \frac{2\pi n}{60} = \frac{2\pi}{T} \tag{21}$$

where T is the spindle revolution period. Let τ be time delay between subsequent teeth, which is given by

$$\tau = \frac{T}{Z_t} = \frac{60}{nZ_t} \tag{22}$$

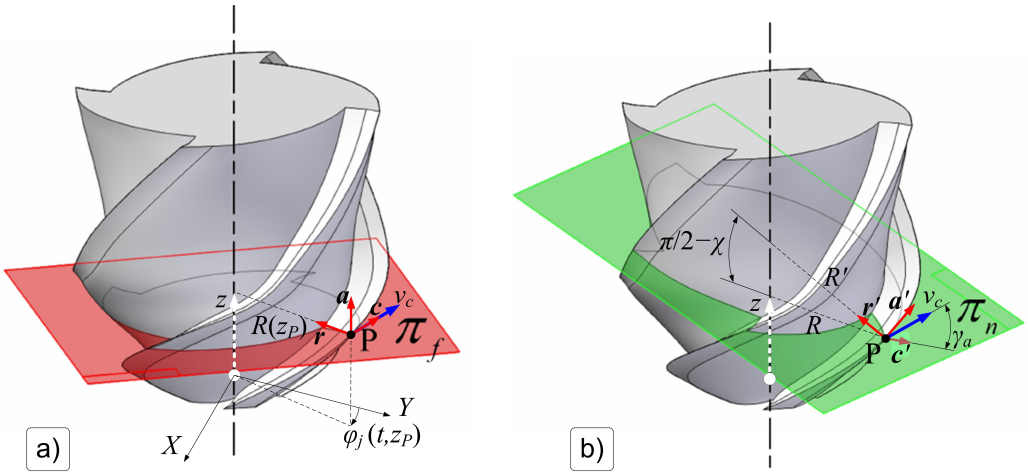

Figure 3: Local reference frames for cutter geometry characterization and cutting force modeling. a) Reference system parallel to working plane π_f. b) Reference system parallel to normal plane π_n.

Let us now focus on the infinitesimal cutting forces acting on the infinitesimal cutting edge length dl located at a generic point P on the j-th flute, as shown in Figure 3.

In cylindrical coordinates P is univocally determined by its height z_P along tool axis, its local radius $R(z_P)$ and its local feed motion angle

$$\varphi_j(t, z_P) \tag{23}$$

which is expressed with respect to the stationary, non rotating reference frame $OXYZ$.

Under the hypothesis of equally spaced teeth we have

$$\varphi_j(t, z) = \varphi_1(t, z) - (j-1)\Delta\varphi_z, \quad j = 1, 2, \ldots, Z_t \tag{24}$$

where $\Delta\varphi_z$ is the angular pitch (angular delay) between subsequent teeth, which is given by

$$\Delta\varphi_z = \frac{2\pi}{Z_t} \tag{25}$$

In order to compute the angular position of the cutter, it is possible to consider the feed motion angle of the first flute tip as main reference, which will be simply denoted by φ in the following, i.e.

$$\varphi(t) = \varphi_1(t, z = 0) \tag{26}$$

The engagement of each tooth part in the workpiece will be described through the window function g_j, as follows

$$g_j(t, z) = g(\varphi_j(t, z)) = \begin{cases} 1 & \text{if } \varphi_{in} < \varphi_j < \varphi_{out} \\ 0 & \text{elsewhere} \end{cases} \tag{27}$$

being φ_{in} and φ_{out} the entrance and exit angles, respectively, recalling that $\varphi_j \in [0, 2\pi]$.

Let us further introduce the following notation

$$\begin{cases} s_j(t, z) = \sin(\varphi_j(t, z)) \\ c_j(t, z) = \cos(\varphi_j(t, z)) \end{cases} \tag{28}$$

Let us now consider the working plane π_f passing through P, which is perpendicular to tool axis and parallel to the stationary plane OXY. This plane does also contain the direction of the local cutting speed v_c. It is possible to define a local reference frame cra, where the unit vector c is parallel to the tangential cutting speed v_c, r is the radial unit vector and a is the axial unit vector parallel to tool axis.

Under generic conditions, the cutting edge may be inclined. Its orientation is univocally determined by the local working cutting edge angle χ (or by its complementary angle $\psi = \pi/2 - \chi$) and by the local axial rake or helix angle γ_a.

The rotation of the reference system cra of an angle equal to χ around the c direction yields a new radial unit vector r'. After another rotation of the new reference frame of an angle equal to γ_a around r', the final $c'r'a'$ reference frame is obtained, which will be important for the oblique cutting force model described in the following.

It is worth noting that the local cutting edge angle χ may in general vary along the cutting edge, even for face shoulder cutters having a nominal $\chi_1 = 90°$, because of the nose radius r_ε.

Similarly, the axial rake angle γ_a may also vary along the cutting edge.

Under an infinitesimal variation dz along the j-th flute, the true cutting edge length is given by

$$dl = \frac{dz}{\sin\chi \cos\gamma_a} \tag{29}$$

Another important quantity is the projection of dl on the ra plane, that is

$$db = dl \cos\gamma_a = \frac{dz}{\sin\chi} \tag{30}$$

For the sake of cutting force modeling it is better to take b as the main curvilinear abscissa, i.e.

$$z \to b\,(z) \tag{31}$$

Accordingly, let us consider an infinitesimal (projected) cutting edge length db located at b, where the instantaneous chip thickness is

$$h_j = h_j\,(t, b) \tag{32}$$

while the infinitesimal chip cross section area is given by

$$dA_j\,(b) = h_j\,(t, b)\,db \tag{33}$$

As stated above, in general

$$\chi = \chi\,(b) \quad \text{and} \quad \gamma_a = \gamma_a\,(b) \tag{34}$$

However, the b dependence as well as the time dependence of other variables will be often omitted in the following in order to simplify notation.

A linear cutting force model is adopted, which was inspired by modern Shearing & Ploughing cutting force models incorporating oblique cutting principles, as those quoted in section 2. Infinitesimal cutting forces acting on the infinitesimal cutting edge db are mainly due to chip pressure on rake face (shearing terms) and dynamic Coulomb friction between the main clearance and the machined surface (ploughing terms). Specifically, the chip pressure on rake face causes:

- a force approximately perpendicular to rake face (i.e. parallel to the c' direction), represented by $k_{cs}dA_j$;
- a force approximately parallel to rake face and perpendicular to the cutting edge along the r' direction, represented by $k_{ns}dA_j$.

At the same time, the dynamic Coulomb friction between the main clearance and the machined surface causes the following ploughing terms:

- a force perpendicular to clearance, i.e. practically parallel to the r' direction, which is represented by $k_{np}db$ term;
- a force parallel to the relative motion direction represented by c or v_c, which is given by $k_{cp}db$. As a consequence, this force has a non-zero projection on both c' and a' directions.

Accordingly, the infinitesimal forces acting on db in the $c'r'a'$ reference system are

$$\begin{cases} dF_{c',j} \cong k_{cs}dA_j + k_{cp}\cos\gamma_a db \\ dF_{r',j} \cong k_{ns}dA_j + k_{np}db \\ dF_{a',j} \cong k_{cp}\sin\gamma_a db \end{cases} \tag{35}$$

The above physical considerations based on this simple Coulomb friction model suggest the following prediction

$$\frac{k_{ns}}{k_{cs}} \approx \frac{k_{cp}}{k_{np}} \approx 0.1 \div 1 \tag{36}$$

which was experimentally confirmed by the S&P coefficients estimated in technical literature [25][53][54], which are approximately within the following

ranges

$$\begin{array}{l} k_{cs} = (0.8 \pm 0.2)\, k_s; \quad k_{ns} = (0.45 \pm 0.3)\, k_{cs}; \\ k_{np} = (0.05 \pm 0.04)\, k_{cs}; \quad k_{cp} = (0.6 \pm 0.35)\, k_{np} \end{array} \tag{37}$$

where k_s is the cutting pressure F_c/A; k_s, k_{cs} and k_{ns} are expressed in [N/mm^2], while k_{cp} and k_{np} are expressed in [N/mm].

It has to be noticed that the dynamic ploughing terms responsible for process damping [27][48] were not considered here, since process damping was neglected in this treatment. However, process damping terms can be easily included in future extensions of this model.

After reference system rotation of γ_a around r' and of χ around c direction, the force components in the cra reference system can be obtained, as follows

$$\begin{cases} dF_{c,j} \cong k_{cs} dA_j \cos\gamma_a + k_{cp} db \\ dF_{r,j} \cong k_{ns} dA_j \sin\chi + k_{np} db \sin\chi + k_{cs} dA_j \sin\gamma_a \cos\chi \\ dF_{a,j} \cong k_{ns} dA_j \cos\chi + k_{np} db \cos\chi - k_{cs} dA_j \sin\gamma_a \sin\chi \end{cases} \tag{38}$$

It is worth noting that the proposed model is able to take into account oblique cutting conditions which may occur when the axial rake $\gamma_a \neq 0$. In these circumstances, the new term $k_{cs} dA_j \sin\gamma_a$ arises, which may especially affect the radial and axial cutting forces.

These forces can be projected along the stationary, non-rotating reference system $OXYZ$, yielding

$$\begin{cases} dF_{x,j} = -dF_{c,j} c_j - dF_{r,j} s_j \\ dM_{y,j} = -dF_{a,j} R s_j \\ dF_{y,j} = dF_{c,j} s_j - dF_{r,j} c_j \\ dM_{x,j} = dF_{a,j} R c_j \end{cases} \tag{39}$$

where it should be recalled that all the terms depend on (t, b), except the radius R which does only depend on b.

After integration along each cutting edge and addition of all the contributions from each tooth, the resultant cutting force components and momenta

are eventually obtained

$$\begin{cases} F_x(t) = \sum_{j=1}^{Z_t} \int_0^{B_j} dF_{x,j}(t,b) \\ M_y(t) = \sum_{j=1}^{Z_t} \int_0^{B_j} dM_{y,j}(t,b) \\ F_y(t) = \sum_{j=1}^{Z_t} \int_0^{B_j} dF_{y,j}(t,b) \\ M_x(t) = \sum_{j=1}^{Z_t} \int_0^{B_j} dM_{x,j}(t,b) \end{cases} \tag{40}$$

3.4. Cutter-workpiece dynamic interaction

Tool tip vibrations perturb the instantaneous local chip thickness as follows

$$h_j(t,b) = \underbrace{h_{j0}(t,b)}_{\text{nominal},\tau-\text{periodic}} + \underbrace{h_{j\delta}(t,b)}_{\substack{\text{regenerative} \\ \text{perturbation}}} \tag{41}$$

where the instantaneous nominal chip thickness h_{j0} is given by

$$h_{j0}(t,b) \cong g_j(t,b)\, f_z s_j(t,b) \sin\chi(b) \tag{42}$$

being f_z the feed per tooth.

The regenerative perturbation is classically given by

$$h_{j\delta}(t,b) = [u_r(t) - u_r(t-\tau)] \sin\chi(b) \tag{43}$$

where u_r is the transverse vibration projected in the radial direction of the j^{th} tooth.

Nevertheless, when axial vibrations cannot be neglected, new terms arise in the regenerative chip thickness formula, i.e.

$$h_{j\delta}(t,b) = [u_r(t) - u_r(t-\tau)] \sin\chi(b) - [u_a(t) - u_a(t-\tau)] \cos\chi(b) \tag{44}$$

as illustrated in Figure 4.

In short, this new theoretical result explains the influence of axial vibrations on regenerative chip thickness and thus on process stability.

In the current case, by accepting the coupling between radial and axial vibrations expressed by Equations (10) and (11) we finally get

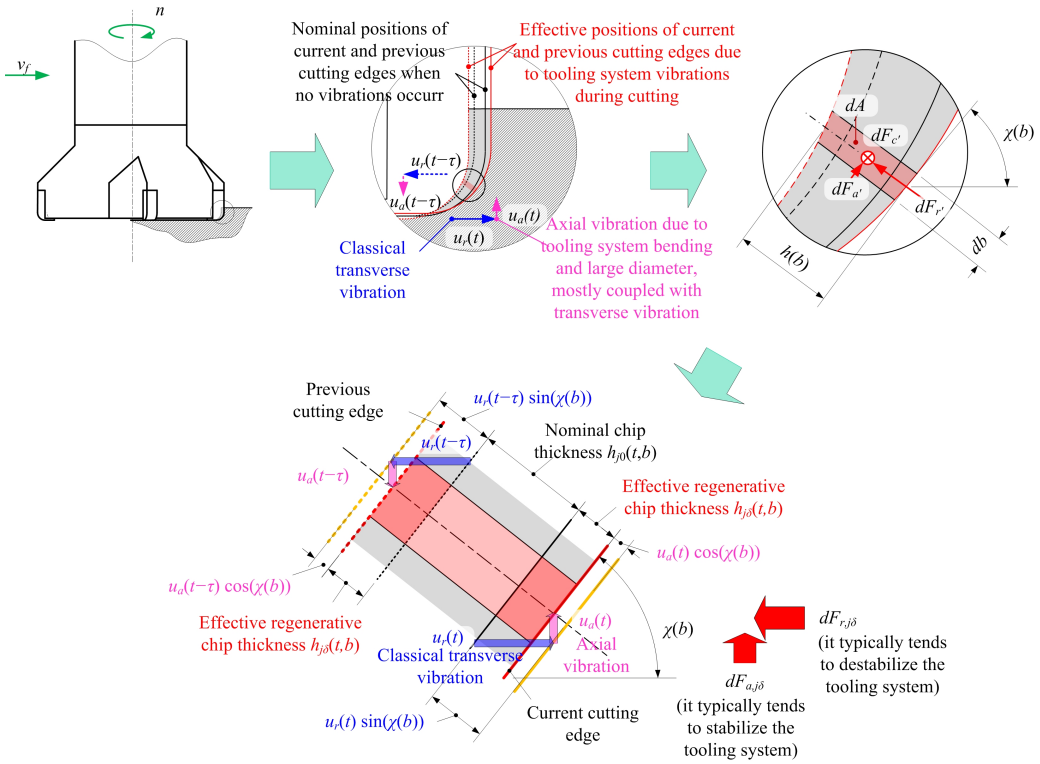

Figure 4: Schematic representation of regenerative chip thickness behavior on inclined cutting edges, showing the dependence on both radial and axial vibrations.

$$h_{j\delta}(t,b) = [\sin\chi(b) - \cos\chi(b)\, R(b)\, \nu]\,[u_r(t) - u_r(t-\tau)] \tag{45}$$

where $R(b)$ is the local radius at the considered abscissa b.

By comparing the new term with the classical term, it yields

$$\frac{\text{new term}}{\text{classical term}} = \frac{\cos\chi R\nu}{\sin\chi} = \operatorname{cotg}\chi\frac{3D}{4L} \tag{46}$$

For example, by considering a possible (not so unlikely) situation with

$$\frac{D}{L} \approx \frac{1}{3}, \quad \chi \approx 45^\circ \quad \Rightarrow \frac{\text{new term}}{\text{classical term}} \approx 25\% \tag{47}$$

which represents a considerable variation with respect to the classical result, which will significantly affect the predicted stability lobes.

Let us now generalize the above result to the 3D milling case. By following the equations introduced in subsection 3.2, one may eventually obtain

$$\begin{aligned} h_{j\delta}(t,b) = &\underbrace{h_{j\delta,ux}(t,b)}_{\tau-\text{periodic}}\underbrace{[u_x(t)-u_x(t-\tau)]}_{\text{regenerative perturbation}}+ \\ &+\underbrace{h_{j\delta,uy}(t,b)}_{\tau-\text{periodic}}\underbrace{[u_y(t)-u_y(t-\tau)]}_{\text{regenerative perturbation}} \end{aligned} \tag{48}$$

where

$$\begin{cases} h_{j\delta,ux}(t,b) = g_j(t,b)\, s_j(t,b)\,[\sin\chi(b) - \cos\chi(b)\, R(b)\,\nu_y] \\ h_{j\delta,uy}(t,b) = g_j(t,b)\, c_j(t,b)\,[\sin\chi(b) - \cos\chi(b)\, R(b)\,\nu_x] \end{cases} \tag{49}$$

It is now possible to linearize cutting forces with respect to the "static", periodic chip thickness h_{j0}, thus yielding

$$\begin{aligned} dF_{w,j}(t,b) &= dF_{w,j}(h_{j0}(t,b)) + \frac{\partial dF_{w,j}}{\partial h_j}(h_{j0}(t,b))\, h_{j\delta}(t,b) = \\ &= dF_{w,j0}(t,b) + dF_{w,j\delta}(t,b) \end{aligned} \tag{50}$$

where w is a generic subscript, the first term is due to the nominal chip thickness, while the force perturbation derives from the regenerative effect.

By differentiating Equation (38), the following relations are obtained

$$\begin{cases} dF_{c,j\delta} = k_{cs} h_{j\delta} \cos\gamma_a db \\ dF_{r,j\delta} = k_{ns} h_{j\delta} \sin\chi db + k_{cs} h_{j\delta} \sin\gamma_a \cos\chi db \\ dF_{a,j\delta} = k_{ns} h_{j\delta} \cos\chi db - k_{cs} h_{j\delta} \sin\gamma_a \sin\chi db \end{cases} \tag{51}$$

Eventually, the force perturbations in the $OXYZ$ stationary reference frame can be deduced from Equations (39) and (48), and they can be rewritten in the following form

$$\begin{bmatrix} dF_{x,j} \\ dM_{y,j} \\ dF_{y,j} \\ dM_{x,j} \end{bmatrix} = \begin{bmatrix} dF_{x,ux} & dF_{x,uy} \\ dM_{y,ux} & dM_{y,uy} \\ dF_{y,ux} & dF_{y,uy} \\ dM_{x,ux} & dM_{x,uy} \end{bmatrix} \begin{bmatrix} u_x(t) - u_x(t-\tau) \\ u_y(t) - u_y(t-\tau) \end{bmatrix} \tag{52}$$

where

$$\begin{cases} dF_{x,ux} = -\left(k_{cs} h_{j\delta,ux} \cos\gamma_a db\right) c_j - \left(k_{ns} h_{j\delta,ux} \sin\chi db + k_{cs} h_{j\delta,ux} \sin\gamma_a \cos\chi db\right) s_j \\ dM_{y,ux} = -\left(k_{ns} h_{j\delta,ux} \cos\chi db - k_{cs} h_{j\delta,ux} \sin\gamma_a \sin\chi db\right) R s_j \\ dF_{y,ux} = \left(k_{cs} h_{j\delta,ux} \cos\gamma_a db\right) s_j - \left(k_{ns} h_{j\delta,ux} \sin\chi db + k_{cs} h_{j\delta,ux} \sin\gamma_a \cos\chi db\right) c_j \\ dM_{x,ux} = \left(k_{ns} h_{j\delta,ux} \cos\chi db - k_{cs} h_{j\delta,ux} \sin\gamma_a \sin\chi db\right) R c_j \end{cases} \tag{53}$$

and $h_{j\delta,ux}$ is now estimated from Equation (49) which includes the effect of axial vibrations arising from tooling system deflection.

Similarly, $dF_{x,uy}$, $dM_{y,uy}$, $dF_{y,uy}$ and $dM_{x,uy}$ can be obtained by substituting $h_{j\delta,ux}$ with $h_{j\delta,uy}$ in Equation (53).

Again, after integration along each cutting edge and summation of all the contributions according to Equation (40), the resultant is

$$\mathbf{F}(t) = \mathbf{F}_0(t) + \mathbf{F}_\delta(t) = \underbrace{\mathbf{F}_0(t)}_{\substack{4\times1 \text{ vector} \\ T \text{ or } \tau-\text{periodic}}} + \underbrace{\mathbf{F'}_1(t)}_{\substack{4\times2 \text{ matrix} \\ T \text{ or } \tau-\text{periodic}}} \underbrace{(\mathbf{u}(t) - \mathbf{u}(t-\tau))}_{\substack{2\times1 \text{ column vector} \\ \text{regenerative vibration}}} \quad (54)$$

where $\mathbf{F}_0$ is the "static" contribution due to the nominal chip thickness and $\mathbf{F}_\delta$ is the "dynamic" term due to the regenerative effect. The matrix $\mathbf{F}'_1$ is T or τ-periodic, depending on whether teeth radial run-out is negligible or not, respectively.

Let us consider a state space form (in the time domain) equivalent to Equation (2), i.e.

$$\begin{cases} \frac{d\mathbf{q}}{dt}(t) = \mathbf{A_W q}(t) + \mathrm{B_W F}(t) \\ \mathbf{u}(t) = \mathbf{C_W q}(t) \end{cases} \quad (55)$$

where $\mathbf{q}$ is the state vector (with d state variables), $\mathrm{A_W}$, $\mathrm{B_W}$, $\mathrm{C_W}$ are the state space matrices representing a time realization of the transfer function $\mathbf{W}(j\omega)$, $\mathbf{F}$ is the input (force) 4×1 vector and $\mathbf{u}$ is the output (displacement) 2×1 vector of the tool tip at time t. Time realization is chosen such that tool tip vibrations along X and Y directions can be directly derived from the first two state space variables, that is

$$\begin{cases} u_x = q_1 \\ u_y = q_2 \end{cases} \quad (56)$$

This is achieved when the output matrix of the adopted time realization is

$$\mathbf{C_W} = \begin{bmatrix} 1 & 0 & 0 & \cdots & 0 \\ 0 & 1 & 0 & \cdots & 0 \end{bmatrix} \quad (57)$$

This choice is particularly important in order to allow monodromy matrix size reduction before eigenvalues computation.

Then the system (55) can be rewritten in the final form

$$\begin{cases} \frac{d\mathbf{q}}{dt} = \mathbf{A}(t)\,\mathbf{q}(t) + \mathbf{B}(t)\,\mathbf{q}(t-\tau) + \mathbf{B}_0(t) \\ \mathbf{u}(t) = \mathbf{C q}(t) \end{cases} \quad (58)$$

where $\mathbf{A}(t)$ and $\mathbf{B}(t)$ are T or τ-periodic $d \times d$ matrices and $\mathbf{B}_0$ is a T or τ-periodic $d \times 1$ column vector. Under the above assumptions, such matrices and vectors are piecewise $\mathcal{C}^1$.

This is a system of linear, periodic Delay Differential Equations which can be efficiently solved by the Chebyshev Collocation Method, as recalled in the next section.

The total vibration $\mathbf{q}(t)$ is generally interpreted as the sum of "static" forced vibrations due to $\mathbf{B}_0(t)$ and "dynamic" regenerative vibrations arising from the difference $(\mathbf{q}(t) - \mathbf{q}(t-\tau))$.

Under the hypothesis of constant speed machining, these terms can be studied separately by applying the superposition principle. Since the forced term is always stable, the whole stability will depend on the regenerative term, which is only influenced by $\mathbf{A}(t)$ and $\mathbf{B}(t)$.

4. Stability analysis

For a given combination of spindle speed and depth of cut, system stability was assessed by considering the general stability criteria of Delay Differential Equations theory [55].

Basically, the discretization method adopted for stability evaluation approximates the infinite-dimensional monodromy operator $\mathbf{U}_g$ representing the Delay Differential Equations system (58) (depurated from the periodic forced excitation $\mathbf{B}_0(t)$) with a finite-dimensional transition matrix $\hat{\mathbf{U}}_g$. The stability of the system depends on the largest matrix eigenvalue, according to the following stability criterion

$$\max\left\{|\lambda_i| : \lambda_i \in \sigma\left(\hat{\mathbf{U}}_g\right)\right\} \cong \rho < 1 \tag{59}$$

where ρ is the spectral radius of the original monodromy operator and λ_i are the eigenvalues of $\hat{\mathbf{U}}_g$.

The monodromy matrix $\hat{\mathbf{U}}_g$ is obtained from a discretization algorithm based on the Chebyshev Collocation Method [55][56][57].

The monodromy matrix size (number of columns = number of rows) is

$$D\left(\hat{\mathbf{U}}_g\right) = 2K(N+1) + d - 2 \tag{60}$$

where d is the dimension of the state space vector $\mathbf{q}(t)$, K is the number of subintervals composing the fundamental interval $[0, \tau]$ where the matrixes

$\mathbf{A}(t)$ and $\mathbf{B}(t)$ are of class $\boldsymbol{\mathcal{C}}^1$, and $N+1$ is the number of Chebyshev collocation points for each subinterval [17]. When the number of collocation points becomes sufficiently high, the spectral radius estimate converges to the theoretical value, as shown in [17]. The algorithm was developed in the MathWorks MATLAB environment, and it was adapted and improved from the ddec MATLAB suite which was originally available on-line at [58]. Further technical details can be found in the above references.

5. Experimental validation

Experimental validation of the new dynamic milling model consisted of three different phases:

1. identification of machining system dynamics through impact testing;
2. estimation of cutting force coefficients by performing dedicated cutting test;
3. determination of experimental stability lobes by performing chatter tests and comparison with model predictions.

5.1. General experimental setup

All the experimental tests were carried out on a 4 axes Mandelli M5 Milling Machine with a horizontal spindle at MUSP laboratory in Piacenza, Italy. The machine is equipped with a Capellini hydrostatic electrospindle (maximum spindle torque T_s=158Nm, maximum achievable spindle speed $n = 8000$ rpm).

The machine tool is equipped with several sensors for monitoring machining vibrations, such as a triaxial accelerometer mounted inside the spindle housing (DYTRAN 3263 - sensitivity 100mV/g) and two orthogonal eddy-current sensors (KEYENCE EX 305V) measuring the relative displacement between the spindle housing and the rotating shaft along X and Y directions.

All sensor signals were sampled at 5000Hz by a National Instruments Data Acquisition device (NI-PXI 1042 Q) and stored on a PC for further analysis, which was carried out in the MathWorks MATLAB environment.

A Kistler dynamometer (9255b coupled with the amplifier 5070A) was used for cutting force measurements during the preliminary milling tests.

Cutting test were performed with a modular tooling system composed of a special spindle adapter (type HSK80A-345-C8-3905/484-100 120 648055), a tool extender module (Sandvik Coromant C8 391.04-80 100), a cutter holder (C8 39105 C12660) and a tailored made face shoulder cutter (Sandvik Coromant TM390-550756). The cutter diameter was $D = 80$ mm, the nominal working cutting edge angle was $\chi_1 = 90°$, the nominal axial rake angle was $\bar{\gamma}_a \approx 10°$ and the tool had four equally spaced teeth ($Z_t = 4$). In these conditions the total tool overhang, from cutter tip to the spindle nose was about $L = 300$ mm.

All the cutting tests were carried out with this tooling system setup. In order to validate the proposed model, cutting inserts with different nose radii

were used. Specifically, three Sandvik Coromant geometries were applied: R390-170404E-PM 4240 ($r_\varepsilon = 0.4$ mm), R390-170408M-PM 4240 ($r_\varepsilon = 0.8$ mm) and R390-1704020M-PM 4240 ($r_\varepsilon = 2$ mm).

In all cases the workpiece material was Ck45 carbon steel, with about 190HB.

5.2. Identification of machining system dynamics

In the first phase, modal analysis was carried out on the tooling system described in the previous subsection, by means of pulse testing technique [59]. The machine dynamics were excited by means of a instrumented hammer and the vibrations were measured through accelerometers and non-contact inductive displacement sensors.

Specifically, eddy current sensors (Keyence EX 110V and Micro-Epsilon type ES1, both with sensitivity ≈ 10 mV/μm) were respectively used for measuring cutter vibrations in the transversal directions X and Y, as well as a triaxial piezoelectric accelerometer Kistler type 8763B100 (sensitivity ≈ 50 mV/g) was applied for transversal and axial vibrations of cutter periphery. Axial vibrations measured in different locations were used for estimating the rotational degrees of freedom ϑ_x and ϑ_y, see Figure 5.

Impulsive forces were applied by means of an instrumented impact hammer type Kistler 9724A2000, both in the transversal and axial directions. By so doing, it was possible to apply both forces (F_x,F_y) and momenta (M_x,M_y) to the cutter, in order to completely identify tooling system dynamics. All the tests were repeated after a 90° rotation of the whole tooling (tool and spindle shaft) in order to assess the symmetry of the main spindle system. The results are summarized in Figure 6. It was observed that all transfer functions are independent from main spindle orientation, with good approximation.

The dynamic compliance measured at tool tip cannot be adequately represented by a single harmonic oscillator for each transversal direction, because the relatively stiff tooling system is dynamically coupled to spindle and machine dynamics as studied in [60] and [61].

Therefore, direct transfer functions W_{uxFx} and W_{uyFy} are characterized by several mechanical resonances, which were determined by applying a novel identification technique inspired by Wavelets theory, which is illustrated in [62]. The final modal parameters are listed in Table 1.

As evidenced in Figure 6, there is a good correlation between experimental measurements and interpolating mathematical models. However, the most

interesting result of this phase are the "secondary" transfer functions W_{uM}, $W_{\vartheta F}$ and $W_{\vartheta M}$ which relate the general degrees of freedom of the cutter tip to the general input forces acting on it, as outlined in subsections 3.1 and 3.2.

In the medium frequency range where the dominant resonances are located, the measured transfer functions are almost proportional to the corresponding direct transfer functions, as predicted by Equations (17), (18) and (19).

This correspondence is good along the Y direction, while it is less accurate but still satisfactory along the X direction, where W_{uxMy} and $W_{\vartheta yFx}$ were slightly smaller than expected. Moreoever, some discrepancies affecting all the secondary transfer functions were observed in the low frequency range (below 70 Hz).

Model inaccuracies affecting secondary transfer functions can be easily explained by recalling that the spindle nose was considered as a perfectly rigid constraint by the toy model. The proposed model does not take into account the effect of machine tool structure eigenmodes on tooling system dynamics. However, the effects of these low-frequency resonances on the rotational degrees of freedom ϑ_x and ϑ_y and then on milling dynamics are practically negligible here. Only the correct modeling of the dominant modes - associated to the cantilever beam behavior of the tooling system - are crucial in this context. These effects may become important when very compact tooling systems are considered, and they could be easily included into future extensions of the proposed model.

Eventually, $W_{\vartheta xMx}$ and $W_{\vartheta yMy}$ were disturbed by a bad signal to noise ratio since they were very small, as expected. For this reason, they were not even shown in Figure 6.

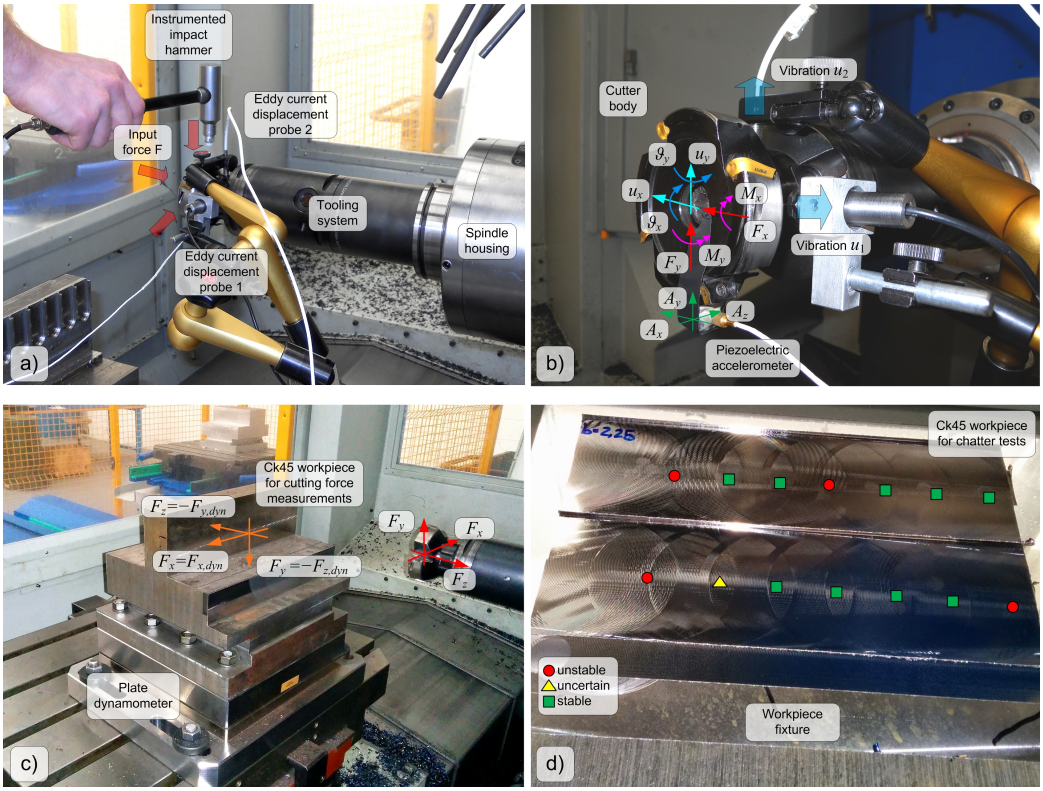

Figure 5: Experimental setup for modal analysis on tooling system - (a) and (b); cutting force measurements (c) and chatter tests (d)

Table 1: Estimated modal parameters of the tooling system under examination.

Dir.	Mode	1	2	3	4	5	6	7	8	9
X	G_k [μm/N]	1.15E-2	3.48E-3	1.29E-2	3.43E-3	3.36E-2	7.39E-3	2.75E-2	9.22E-3	3.96E-3
	f_k [Hz]	28	54.5	72	79.5	260	275.5	327	406.5	453
	ξ_k [ ]	7.34E-2	8.56E-3	4.63E-2	2.71E-2	2.50E-1	5.00E-2	1.17E-1	3.15E-2	2.92E-2
Y	G_k [μm/N]	1.31E-2	2.75E-3	1.90E-2	4.11E-3	4.65E-3	2.26E-2	2.95E-3	1.25E-2	-
	f_k [Hz]	65.5	204	244.5	289	339	392	452.5	700	-
	ξ_k [ ]	1.26E-1	3.68E-2	4.29E-2	4.63E-2	1.08E-1	6.80E-2	2.71E-2	1.00	-

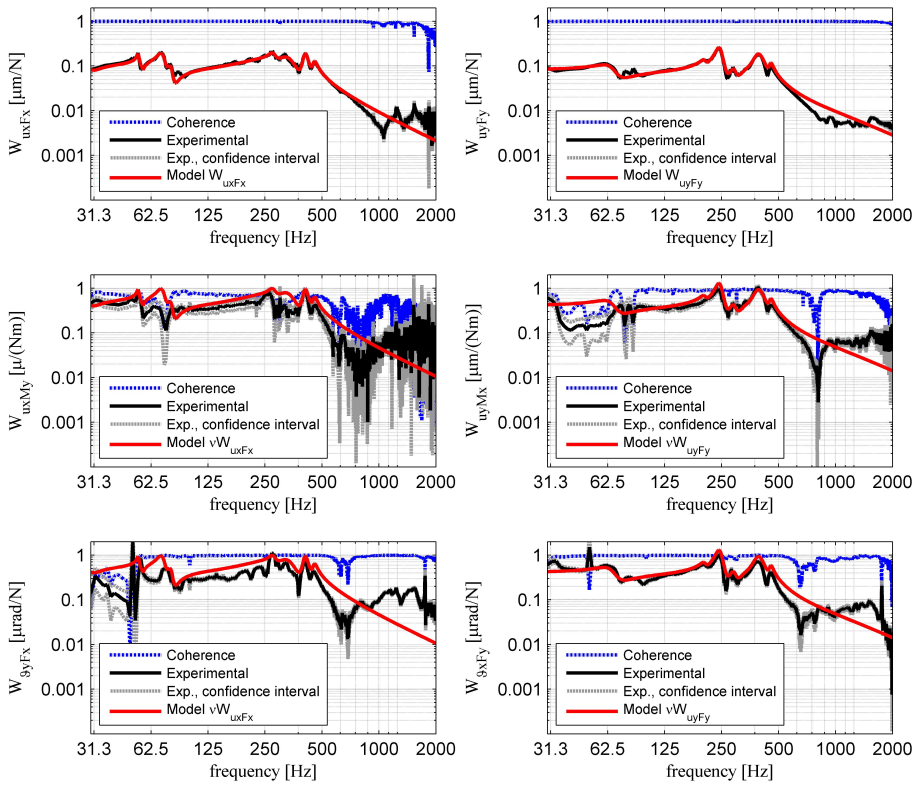

Figure 6: Measured transfer functions of the tooling system and comparison with the proposed model.

5.3. Cutting force model experimental validation

In order to identify and check cutting force model adequacy, several cutting tests were carried out on a Ck45 carbon steel workpiece by using the tooling system described in section 5.1. The workpiece was clamped on a plate dynamometer Kistler type 9255b in order to measure the instantaneous cutting forces exchanged between tool and workpiece, as illustrated in Figure 5 (c).

Different cutting conditions were measured, according to the design of experiments described in Table 2. Specifically, different insert nose radii were tested, as well as different tool-workpiece lateral engagements. The width of cut a_L was about 32 mm for both the pure up milling configuration with $a_{L1} = 40$ mm and the centered configuration with $a_{L1} = 16$ mm.

Table 2: Design of experiments for estimation of cutting force model coefficients

Factor	**Levels**	**Values**
Nose radius r_ε [mm]	2	0.8, 2
Cutter-workpiece lateral position a_{L1} [mm]	1-2	16, 40 (up milling)
Axial depth of cut a_p [mm]	4	0.4, 0.8, 1.6, 2.4
Feed per tooth f_z [mm]	3	0.1, 0.2, 0.25 for $r_\varepsilon = 0.8$ mm; 0.08, 0.14, 0.20 for $r_\varepsilon = 2$ mm
Cutting speed v_c [m/min] (spindle speed n [rpm])	2	200, 350 m/min (800, 1400 rpm)

The dynamics of the plate dynamometer were significantly disturbed by the mechanical resonances of the whole system (machine tool - dynamometer - workpiece). Thus, in order to obtain robust estimates of the S&P coefficients, only average forces were extracted from each measurement and used for the linear regression procedure.

In short, $N = 72$ cutting tests in different cutting conditions were executed, whence a total of $3N = 216$ average force values were collected, see Figure 7. The analysis of the experimental trends confirmed that cutting forces strongly depend on all the independent factors except the cutting speed, whose effect was negligible at first approximation, in accordance with well-known results which can be found in classical literature [63].

The final regression was accomplished by considering the algebraic system

$$\bar{\mathbf{F}}_{exp} = \mathbf{X}\,\mathbf{k} + \varepsilon \tag{61}$$

where the known term was composed by $3N$ rows

$$\bar{\mathbf{F}}_{exp} = \left[\begin{array}{cccccccccc} \bar{F}_{x1} & \cdots & \bar{F}_{xN} & \bar{F}_{y1} & \cdots & \bar{F}_{yN} & \bar{F}_{z1} & \cdots & \bar{F}_{zN} \end{array} \right]^{\mathrm{T}}_{exp} \tag{62}$$

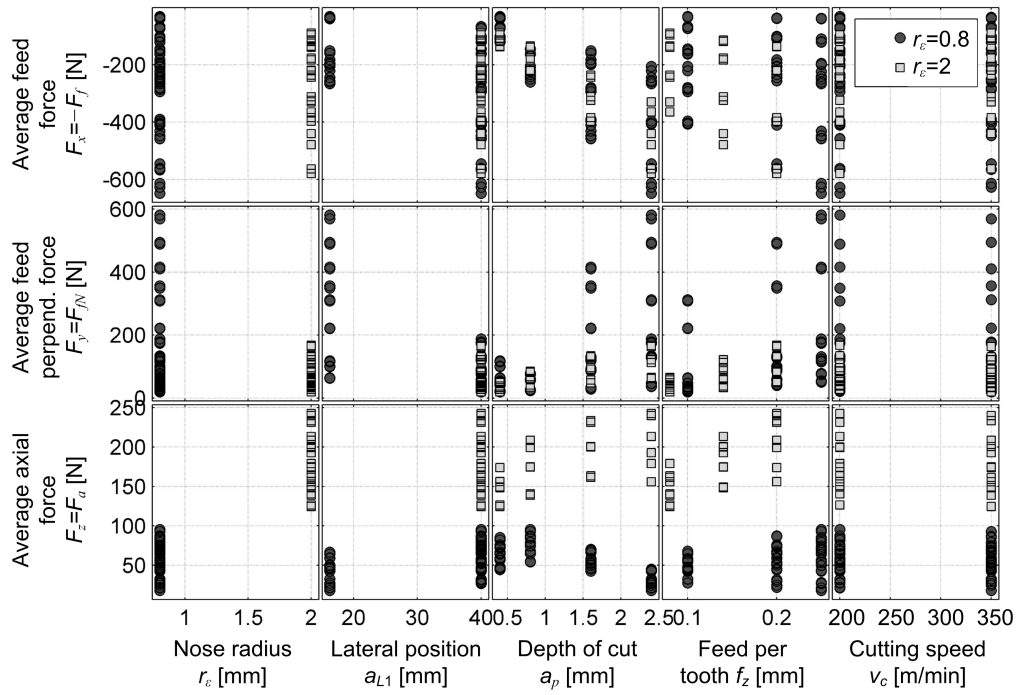

Figure 7: Average experimental forces along the X, Y and Z directions of the stationary reference frame.

while the vector of unknown S&P coefficients was

$$\mathbf{k} = \left[\; k_{cs} \; k_{cp} \; k_{ns} \; k_{np} \; \right]^{\mathrm{T}} \tag{63}$$

Matrix $\mathbf{X}$ is obtained by integrating Equation (40) with respect to time (or equivalently, with respect to the reference feed motion angle φ) for all experimental conditions, by taking into account tool geometry and the different tool-workpiece engagement conditions, as illustrated in Appendix A.

Optimal values of S&P coefficients enclosed into the vector $\mathbf{k}_{opt}$ were determined by the classical pseudo-inverse formula and are listed in Table 3. Accordingly, the average cutting forces estimated by the model were determined as usual

$$\bar{\mathbf{F}}_{mod} = \mathbf{X}\,\mathbf{k}_{opt} \tag{64}$$

Eventually, the relative residues between model estimates and effective

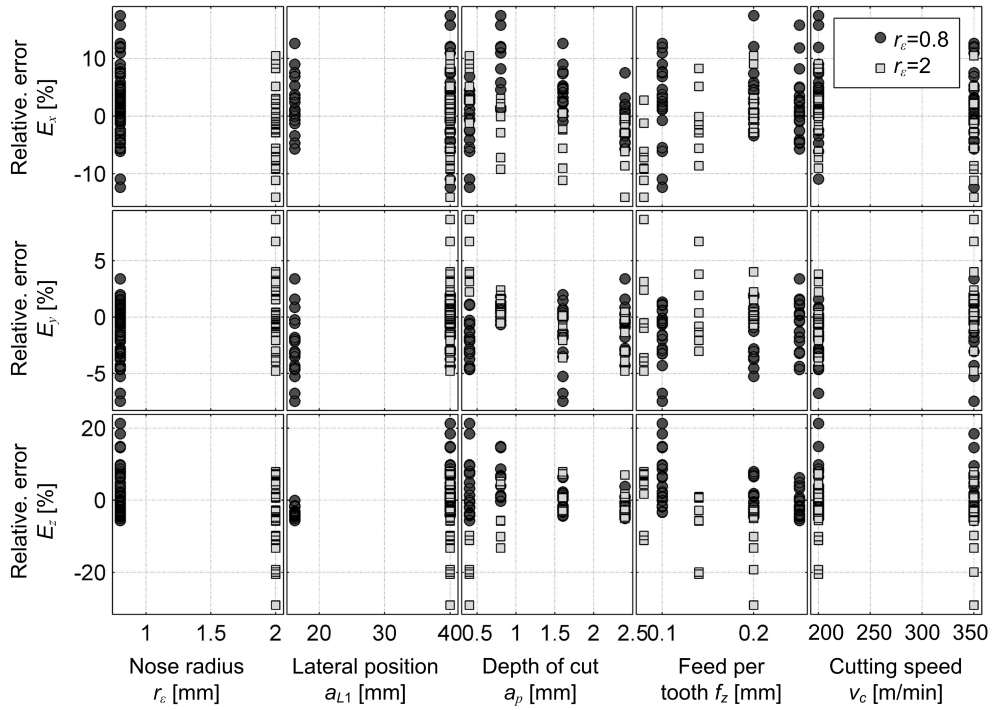

Figure 8: Relative errors between average forces estimated by the adopted model and the effective experimental values, along the X, Y and Z directions of the stationary reference frame.

experimental values were computed, i.e.

$$\varepsilon_{wi} = \frac{\bar{F}_{wi,mod} - \bar{F}_{wi,exp}}{R_{i,exp}} \, [\%] \qquad w = x, y, z; \quad i = 1, \ldots, N \tag{65}$$

where the normalization was carried out by using the modulus of the resultant average force, that is

$$R_{i,exp} = \sqrt{\bar{F}^2_{xi,exp} + \bar{F}^2_{yi,exp} + \bar{F}^2_{zi,exp}} \tag{66}$$

Some indexes for evaluating cutting force model adequacy are listed in Table 4. In conclusion, the obtained model is able to explain most of the variability of the observed cutting force trends by using only 4 coefficients, confirming the effectiveness of modern S&P models inspired by oblique cutting

theory, in comparison to other pure mechanistic/mathematical approaches based on a greater number of coefficients [37][64].

Table 3: Estimated cutting force coefficients

k_{cs} [N/mm^2]	k_{cp} [N/mm]	k_{ns} [N/mm^2]	k_{np} [N/mm]
1657	68	557	102

Table 4: Cutting force model adequacy

Index	X	Y	Z
Squared linear corr. coeff. R^2 []	0.988	0.996	0.923
Standard dev. of rel. error σ [%]	6.1	2.5	7.6
Systematic relative error μ [%]	1.2	-0.6	-0.4

It should be noticed that the behavior of the model is less accurate but still satisfactory along the axial direction. This was likely due to the generally small axial contributions - in comparison to the transverse force components - characterizing this experimental setup and cutting conditions.

5.4. Chatter tests and comparison with model prediction

In order to validate the new model and show its predictive capabilities, two specific experimental campaigns were conceived and carried out. In the first campaign, nose radius was set to $r_\varepsilon = 0.4$ mm, while it was set to 2 mm in the second campaign. Except the nose radius, the tooling system was kept the same during all the tests, as well as the workpiece material.

Slotting conditions were adopted ($a_L/D = 100\%$) in order to allow stability borders identification in a reasonable range of depths of cut, without damaging the machine tool. Feed per tooth was set to 0.2 mm for all the cutting tests.

For each experimental campaign, a grid of cutting parameter combinations was tested, as summarized in Table 5.

As can be observed, the depth of cut was increased by discrete increments from 1.75 mm until severe chatter occurred. The test was stopped at a maximum depth of cut of 3.75 mm if no chatter was observed.

The stability of the system was assessed both from visual inspection and by calculating quantitative chatter indicators [65] obtained from vibration/acceleration signals acquired by the sensors integrated into the spindle housing and described in subsection 5.1.

Table 5: Design of experiments for chatter tests

Factor	**Levels**	**Values**
Nose radius r_ε [mm]	2	0.4, 2
Depth of cut a_p [mm]	7	increments of 0.25 starting from 1.75 up to 3.75
Cutting speed v_c [m/min] (spindle speed n [rpm])	14	increments of 9.6 starting from 200 up to 325 (increments of 38 starting from 800 up to 1294)

The stability analysis was carried out by the Chebyshev Collocation Method recalled in section 4.

In the considered case study there are 9 harmonic oscillators along the X direction and 8 harmonic oscillators along the Y direction, for a total of 17 independent harmonic oscillators included in the tooling system transfer functions, Table 1. Thus, the size of the square matrix $\mathbf{A}$ is $d = 17 \cdot 2 = 34$.

Apparently, the new approach seems to require a greater matrix size d since it introduces new degrees of freedom (ϑ_x and ϑ_y) in addition to the classical displacements u_x and u_y. Nevertheless, it is important to recall that rotational and translational degrees of freedom are different viewpoints of the same eigenmodes. In the current case, they are even assumed proportional to each other thanks to the reasonable assumption (10). Accordingly, the classical model and the new model are based on the same number of independent harmonic oscillators and hence on the same matrix size d. Therefore, the new model significantly improves and refines the classical model by keeping the same computational complexity.

In the case study under interest there are no kinks in the time interval ($K = 1$, Equation (60)) since the angular engagement $\varphi_{out} - \varphi_{in} = \pi$ is a perfect multiple of the angular pitch $\Delta\varphi_z = 2\pi/Z_t = \pi/2$. Some preliminary numerical investigations were performed in order to determine an adequate matrix size $D\left(\hat{\mathbf{U}}_g\right)$ for assuring a good accuracy of the estimated spectral radius. It was assessed that a good accuracy

$$\left|\frac{\hat{\rho} - \rho_{th}}{\rho_{th}}\right| < 0.001\% \tag{67}$$

could be achieved in this case by adopting $D\left(\hat{\mathbf{U}}_g\right) = 128$, which corresponded to a number of Chebyshev collocation points equal to $N + 1 = 48$. The predicted stability lobes were determined by calculating a grid of about 80 spindle speed levels $\times$ 40 depth of cut levels.

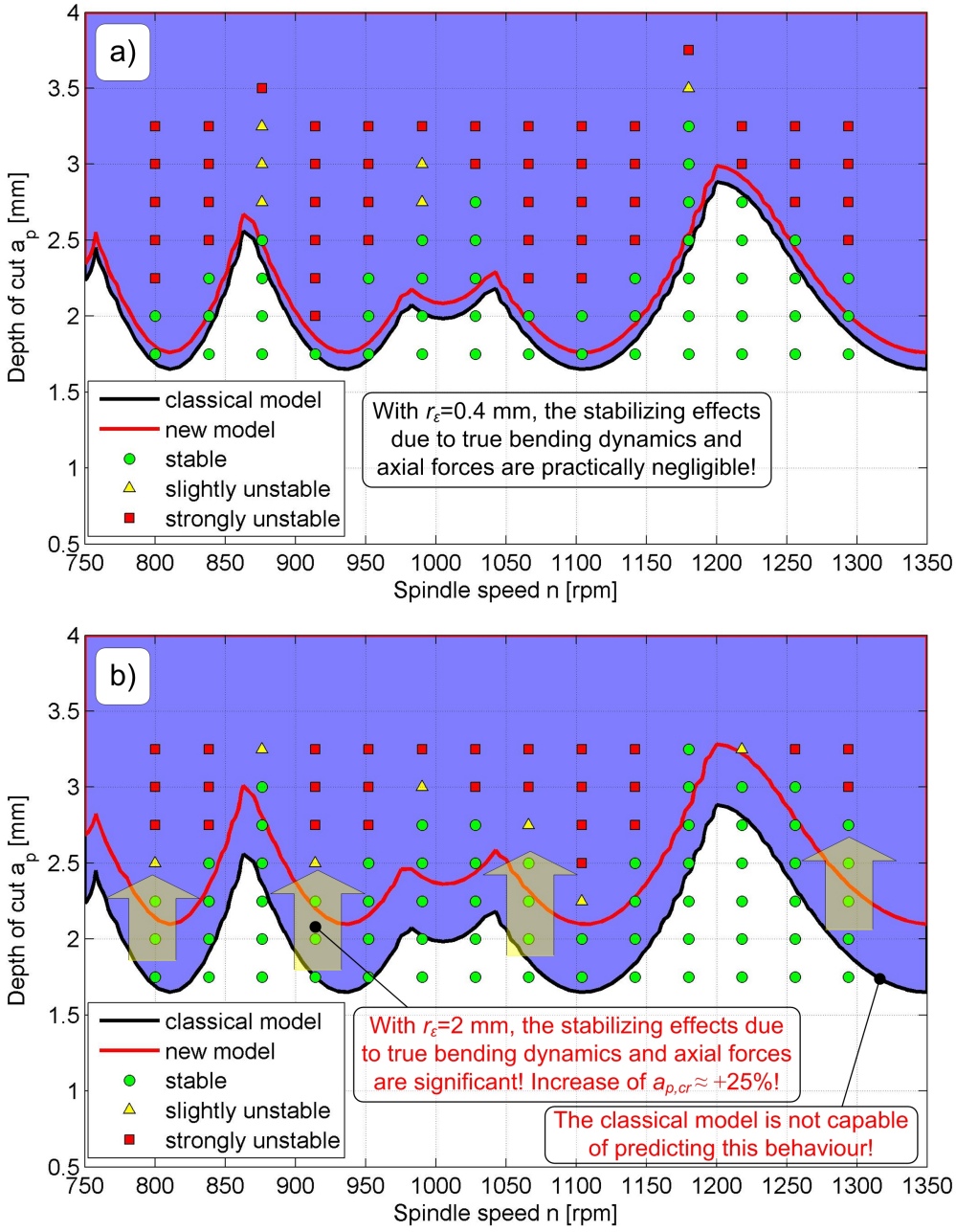

Figure 9: Comparison between experimental and predicted stability lobes.

The obtained results (Figure 9 (a)) evidenced that there is only a slight difference between the classical and the new modeling approaches when $r_\varepsilon = 0.4$ mm. The two stability predictions are very close to each other because the nose radius is too small for highlighting the difference between the classical and the novel approach. In the current case both the predictions do slightly underestimate (about 10%) the effective stability borders. This small discrepancy is acceptable and it can be explained by the uncertainties affecting the identified model coefficients and by other reasonable error sources [25].

However, when the larger nose radius $r_\varepsilon = 2$ mm is used, the experimental stability lobes are considerably different, showing a remarkable increase (about +25%) of the critical depth of cut with respect to the previous case. This shift can now be easily explained by the reduction of the regenerative effect associated to the rotational degrees of freedom (Equation (50)) and by the stabilizing effect of the axial forces (Equation (13)).

Only the new modeling approach predicts a similar shift of the stability borders towards higher depths of cut, though the variation is slightly smaller than the experimental counterpart. On the contrary, the stability borders predicted by the classical approach are unaffected by this change.

The obtained results showed that the new approach is able to significantly improve the accuracy of the predicted stability lobes, thus deepening the understanding of machining chatter.

For achieving this goal, the new model takes into account the effects of cutting edge geometry (here represented by r_ε, χ_1, $\bar{\gamma}_a$), tooling system geometry (D/L), enhanced tooling system dynamics (W_{uM}, $W_{\vartheta F}$ in addition to W_{uF}) and complex cutting mechanics from an innovative perspective.

6. Conclusions

According to the considerations and results presented in this work, we may draw the following conclusions.

In this research work, a revolutionary model was proposed for modeling the true dynamics of tooling systems, especially those characterized by relatively large cutter diameter D in comparison to tool overhang L and by curved or inclined cutting edges with an average working cutting edge angle $\chi < 90°$.

First, the mathematical formulation of the new dynamic model was described in detail. In comparison to state of the art models, the new model

takes into account additional dynamic effects, such as

- the rotational degrees of freedom ϑ_x and ϑ_y which are necessary - together with the classical translational vibrations u_x and u_y - to accurately characterize tooling system deflection in the coordinate planes containing spindle axis.

- the bending momenta M_x and M_y deriving from axial forces applied at cutting inserts.

By including these effects, a new formula for regenerative chip thickness estimation was obtained. A corrective term appears which depends on tooling system aspect ratio D/L and on the local working cutting edge angle χ. In comparison to the classical regenerative chip thickness, this correction is significant even for moderate aspect ratios, as those characterizing many industrial applications (see Equation (47)).

Similarly, the bending momenta associated to axial forces may play an important role for accurately describing the dynamic behavior of the machining system. Axial forces tend to reduce the transverse vibrations by a relative factor depending on tooling system aspect ratio D/L and on the local working cutting edge angle χ (see Equations (13) and (14)).

The new model was experimentally validated by performing tooling system dynamics identification, cutting force coefficient estimation and stability lobes diagram determination.

The results of modal analysis confirmed that the effect of rotational degrees of freedom and the effect of bending momenta deriving from axial forces are in general not negligible. Also, measurements confirmed the approximate proportionality between the additional transfer functions introduced by the new model and the classical, direct transfer functions connecting transverse vibrations to transverse forces.

Even by including the additional degrees of freedom and bending momenta, the increase of mathematical complexity is very limited, since the size of the state space vector is unaffected by this fact. In other words, the new model refines the classical one without requiring additional computational load and elaboration time for stability evaluation.

Eventually, stability lobes diagrams were determined by using the same tooling system with different nose radii, in order to highlight the differences between the proposed and the classical approach. The obtained results confirmed the effectiveness of the new model, which correctly predicted a sig-

nificant shift of the stability borders when a larger nose radius was adopted, while the classical approach was insensitive to this variation.

Accordingly, a strongly innovative model of milling dynamics was conceived and validated. It will be of further interest to evaluate the predictive capabilities of the new theory in many other important industrial cases, where the afore mentioned effects may play a crucial role.

7. Acknowledgements

The Present Research Work has been developed under the moral patronage of the *Machining* division of the Italian Association of Manufacturing Technology - AITeM.

8. References

[1] G. Stepan, Delay-differential equation models for machine tool chatter, Nonlinear Dynamics of Material Processing and Manufacturing, Ed.: F.C. Moon, John Wiley and Sons, New York, (1998), 165-19

[2] Y. Altintas, M. Weck, Chatter stability of metal cutting and grinding, Annals of the CIRP, 53/2 (2004) 619-642

[3] G. Quintana, J. Ciurana, Chatter in machining processes: A review. Int J. Mach Tools Manuf 51 (2011) 363-376

[4] M. Kayhan M, E. Budak, An Experimental Investigation of Chatter Effects on Tool Life. Proc. IMechE, Part B: Journal of Engineering Manufacture, 223 (11) (2009) 1455-1463

[5] S.A. Tobias, W. Fishwick, Theory of Regenerative Chatter, The Engineer, London, (1958).

[6] H.E. Merritt, Theory of Self-Excited Machine Tool Chatter, Trans. ASME Journal of Engineering for Industry, 87 (1965), 447-454

[7] J. Tlusty, Analysis of the state research in cutting dynamics, Annals of the CIRP, 2 (1978)583-589

[8] S. Smith, J. Tlusty, Efficient simulation programs for chatter in milling, CIRP Annals, Manufacturing Technology, 42-1 (1993) 463-466

[9] Y. Altintas, E. Budak, Analytical Prediction of Stability Lobes in Milling, Annals of the CIRP, 44 (1995) 357-362.

[10] M. Sortino, G. Totis, F. Prosperi, Modeling the dynamic properties of conventional and high-damping boring bars, Mechanical Systems and Signal Processing, 34 (2013) 340-352

[11] E. Budak, An Analytical Design Method for Milling Cutters with Non-constant Pitch to Increase Stability, part 2: Application, Journal of Manufacturing Science and Engineering, Trans. ASME, 125 (2003) 35-38

[12] M. Weck, C. Brecher, Werkzeugmaschinen 5: Messtechnische Untersuchung und Beurteilung, dynamische Stabilität (2006), Springer-Verlag

[13] F. Aggogeri, A. Merlo, M. Mazzola, Multifunctional structure solutions for Ultra High Precision (UHP) machine tools, International Journal of Machine Tools and Manufacture, 50/4 (2010) 366-373

[14] D. G. Lee, H-C. Sin, N. P. Suh, Manufacturing of a Graphite Epoxy Composite Spindle for a Machine Tool, CIRP Annals - Manufacturing Technology, 34/1 (1985) 365-369

[15] D. Mei, T. Konga, A.J. Shihb, Z. Chen, Magnetorheological fluid-controlled boring bar for chatter suppression, J. Mater. Process. Technol., 209 (2009) 1861-1870

[16] D.J. Segalman, E.A. Butcher, Suppression of Regenerative Chatter via Impedance Modulation, Journal of Vibration and Control, 6/2 (2000) 243-256

[17] G. Totis, P. Albertelli, M. Sortino, M. Monno, Efficient evaluation of process stability in milling with Spindle Speed Variation by using the Chebyshev Collocation Method, Journal of Sound and Vibration, 333 (2014) 646-668

[18] J.L. Dohner, J.P. Lauffer, T.D. Hinnerichs, N. Shankar, M. Regelbrugge, C.M. Kwan, R. Xu, B. Winterb, Mitigation of Chatter Instabilities by Active Structural Control, Journal of Sound and Vibration, 269 (2004) 197-211

[19] C. Brecher, D. Manoharan, U. Ladra, H.-G. Köpken, Chatter suppression with an active workpiece holder, Prod. Eng. Res. Devel., 4 (2010) 239-245

[20] G.Aguirre, M. Gorostiaga, T. Porchez, J. Munoa, Self-tuning dynamic vibration absorber for machine tool chatter suppression. 28th Annual Meeting of the American Society for Precision Engineering (ASPE), Oct 2013, St. Paul, Minnesota, United States

[21] N.J.M. van Dijk, E.J.J. Doppenberg, R.P.H. Faassen, N. van de Wouw, J.A.J. Oosterling, H. Nijmeijer, Automatic in-process chatter avoidance in the high speed milling process, ASME Journal of Dynamic Systems, Measurement and Control, 132 (2010) 1-14

[22] http://www.okuma.com/machining-navi

[23] J. Gradisek, M. Kalveram, T. Insperger, K. Weinert, G. Stepan, E. Govekar, I. Grabec, On stability prediction for milling, International Journal of Machine Tools and Manufacture, 45 (2005) 768-781

[24] Y. Altintas, G. Stepan, D. Merdol, Z. Dombovari, Chatter stability of milling in frequency and discrete time domain, CIRP Journal of Manufacturing Science and Technology, 1 (2008) 35-44

[25] G. Totis, RCPM - A new method for robust chatter prediction in milling, International Journal of Machine Tools and Manufacture, 49 (2009) 273-284

[26] A. Tobias, Machine Tool Vibration, Blackie and Sons Ltd., (1965)

[27] V. Sellmeier, B. Denkena, High speed process damping in milling, CIRP Journal of Manufacturing Science and Technology, 5 (2012) 8-19

[28] K. Ahmadi, F. Ismail,Stability lobes in milling including process damping and utilizing Multi-Frequency and Semi-Discretization Methods, International Journal of Machine Tools & Manufacture, 54-55 (2012) 46-54

[29] J. Tlusty, Manufacturing Processes and Equipment, Prentice-Hall, Englewood Cliffs, NJ, (2000)

[30] A. Gasparetto, Eigenvalue analysis of mode-coupling chatter for machine tool stabilization, Journal of Vibration and Control, 7/2 (2001) 181-197

[31] X.J. Zhang, C.H. Xiong, Y. Ding, M.J. Feng, Y.L. Xiong, Milling stability analysis with simultaneously considering the structural mode coupling effect and regenerative effect, International Journal of Machine Tools & Manufacture, 53 (2012) 127-140

[32] T. Kalmar-Nagy, F.C. Moon, Mode-Coupled Regenerative Tool Vibrations in: G. Radons, R. Neugebauer (Eds), Nonlinear dynamics of production systems, Berlin, Wiley-VCH Berlin (2006), 129-149.

[33] I. Grabec, Chaotic dynamics of the cutting process, International Journal of Machine Tools and Manufacture, 28 (1988) 19-32

[34] J. Warminski, G. Litak, M.P. Cartmell, R. Khanin, M. Wiercigroch, Approximate analytical solutions for primary chatter in the non-linear metal cutting model, Journal of Sound and Vibration, 259/4 (2003) 917-933

[35] M.A. Davies, T.J. Burns, C.J. Evans, On the dynamics of chip formation in machining hard materials, Annals of the CIRP, 46 (1997)25-30

[36] T.R. Sisson, R.L. Kegg, An explanation of low speed chatter effects, Journal of Engineering for Industry, Transactions of the ASME,(1969) 951-958

[37] Y. Altintas, Manufacturing automation: Metal Cutting Mechanics, Machine Tool Vibrations, and CNC Design, (2000), Cambridge University Press

[38] F.J. Campa, L.N. Lopez de Lacalle, A. Celaya, Chatter avoidance in the milling of thin floors with bull-nose endmills: model and stability diagrams, International Journal of Machine Tools & Manufacture, 51 (2011) 43-53

[39] E. Budak, L.T. Tunc, S. Alan, H.N. Ozguven, Prediction of workpiece dynamics and its effects on chatter stability in milling, CIRP Annals - Manufacturing Technology, 61 (2012) 339-342

[40] Z.M. Kilic, Y. Altintas, Generalized mechanics and dynamics of metal cutting operations for unified simulations, International Journal of Machine Tools & Manufacture, 104 (2016) 1-13

[41] T. Inspergera, G. Stepan, P.V. Bayly, B.P. Mann, Multiple chatter frequencies in milling processes, Journal of Sound and Vibration, 262 (2003) 333-345

[42] B.P. Mann, T. Insperger, P.V. Bayly, G. Stepan,Stability of up-milling and down-milling, part 2: experimental verification, International Journal of Machine Tools & Manufacture, 43 (2003) 35-40

[43] E. Govekar, J. Gradisek, M. Kalveram, T. Insperger, K. Weinert, G. Stepan, I. Grabec, On Stability and Dynamics of Milling at Small Radial Immersion, CIRP Annals, 54/1 (2005) 357-362.

[44] G. Catania, N. Mancinelli, Theoretical-experimental modeling of milling machines for the prediction of chatter vibration, International Journal of Machine Tools & Manufacture, 51 (2011) 339-348

[45] V. Sellmeier, B. Denkena, Stable islands in the stability chart of milling processes due to unequal tooth pitch, International Journal of Machine Tools & Manufacture, 51 (2011) 152-164

[46] G.P. Zou, I. Yellowley, R.J. Seethaler, A new approach to the modeling of oblique cutting processes, International Journal of Machine Tools & Manufacture, 49 (2009) 701-707

[47] M. Wan, W.-J. Pan, W.-H. Zhang, Y.-C. Ma, Y. Yang, A unified instantaneous cutting force model for flat end mills with variable geometries, Journal of Materials Processing Technology, 214 (2014) 641-650

[48] M. Wan, Y.C. Ma, J. Feng, W.H. Zhang, Study of static and dynamic ploughing mechanisms by establishing generalized model with static milling forces, International Journal of Mechanical Sciences, 114 (2016) 120-131

[49] Z. Dombovari, Y. Altintas, G. Stepan,The effect of serration on mechanics and stability of milling cutters, International Journal of Machine Tools & Manufacture, 50 (2010) 511-520

[50] A.R. Yusoff, N.D. Sims, Optimisation of variable helix tool geometry for regenerative chatter mitigation, International Journal of Machine Tools & Manufacture, 51 (2011) 133-141

[51] G. Stepan, J. Munoa, T. Insperger, M. Surico, D. Bachrathy, Z. Dombovari, Cylindrical milling tools: Comparative real case study for process stability, CIRP Annals - Manufacturing Technology, 63 (2014) 385-388

[52] G. Genta, Dynamics of Rotating Systems, (2005), Springer

[53] M. Sortino, G. Totis, F. Prosperi, Development of a practical model for selection of stable tooling system configurations in internal turning, International Journal of Machine Tools & Manufacture, 61 (2012) 58-70

[54] G. Totis, M. Sortino, Robust Analysis of Stability in Internal Turning, Procedia Engineering, 69 (2014) 1306-1315

[55] E. Bueler, Chebyshev Collocation for Linear, Periodic, Ordinary and Delay Differential Equations: a Posteriori Estimates, (2004), Cornell University Library, http://arxiv.org/, math.NA/0409464

[56] E. Bueler, E. Butcher, Stability of periodic linear delay-differential equations and the Chebyshev approximation of fundamental solutions, UAF Dept. of Mathematical Sciences Technical Report 2002-2003

[57] L.N. Trefethen, Spectral Methods in MATLAB, (2000), SIAM Press, Philadelphia

[58] http://www.cs.uaf.edu/

[59] D.J. Ewins, Modal Testing: Theory, Practice and Application 2nd Edition, ISBN: 978-0-86380-218-8 (2009) Wiley

[60] P. Albertelli, N. Cau, G. Bianchi, M. Monno, The effect of dynamic interaction between machine tool subsystems on cutting process stability, TInt. J. Adv. Manuf. Technol., 58 (9-12) (2012) 923-932

[61] P. Kolar, M. Sulitka, M. Janota, Simulation of dynamic properties of a spindle and tool system coupled with a machine tool frame, Int. J. Adv. Manuf. Technol., 54/1 (2011) 11-20

[62] G. Totis, M. Sortino, S. Belfio, Wavelet-like analysis in the frequency-damping domain for modal parameters identification, 26-th DAAAM International Symposium on Intelligent Manufacturing and Automation, Proceedings of the 26th DAAAM International Symposium, Wien (2016), 580-588, DOI: 10.2507/26th.daaam.proceedings.079

[63] G.F. Micheletti, Tecnologia Meccanica 1 - Il Taglio dei Metalli, (1977), UTET, Torino

[64] Y.C. Kao, N.T. Nguyen, M.S. Chen, S.C. Huang, A combination method of the theory and experiment in determination of cutting force coefficients in ball-end mill processes, Journal of Computational Design and Engineering, 2 (2015) 233-247

[65] E. Kuljanic, M. Sortino, G. Totis, Multisensor approaches for chatter detection in milling, Journal of Sound and Vibration, 312 (2008) 672-693.

9. Appendix A - Average cutting force equations

For the sake of completeness and clarity the formulas used for cutting force coefficients identification are given below.

Average cutting forces are given by

$$\bar{F}_w = \frac{1}{T}\int_0^T F_w(t)\,dt = \frac{1}{2\pi}\int_0^{2\pi} F_w(\varphi)\,d\varphi, \quad w = x, y, z \tag{68}$$

where the last equality holds since we are considering a conventional milling operation performed with constant spindle speed, which is characterized by

$$\varphi(t) = \varphi_1(t, b_1 = 0) = \Omega t \tag{69}$$

where we recall that (φ_1, b_1) are the cylindrical coordinates of a generic point on the first cutting flute. It is straightforward to see that

$$\bar{F}_w = Z_t\left[\frac{1}{2\pi}\int_0^{2\pi} d\varphi \int_0^{B_1} dF_{w,1}(\varphi, b_1)\, g_1(\varphi, b_1)\, db_1\right] \qquad w = x, y, z \tag{70}$$

where the total average force is simply Z_t times the contribution deriving from the first tooth. The double integral symbol stands for the feed motion angle φ running from 0 to 2π and the projected cutting edge abscissa b_1 running from 0 to the total cutting edge length B_1 corresponding to the selected the depth of cut a_p.

Thanks to the presence of the window function g_1 it is possible to strongly simplify the whole calculation by performing the following variable substitution

$$(\varphi, b_1) \rightarrow (\varphi_1, b_1) \Rightarrow \bar{F}_w = Z_t\left[\frac{1}{2\pi}\int_{\varphi_{in}}^{\varphi_{out}} d\varphi_1 \int_0^{B_1} dF_{w,1}(\varphi_1, b_1)\, db_1\right] \quad w = x, y, z \tag{71}$$

where the action of the window function is represented by the new integral limits φ_{in} and φ_{out}.

Thus, by applying the formulas introduced in section 3.3, after some

algebraic manipulation one obtains

$$\begin{aligned}\bar{F}_x = &\left(-\frac{Z_t}{2\pi}\iint f_z s_1 c_1 \sin\chi\cos\gamma_a\, db_1\, d\varphi_1\right) k_{cs}+\\ &+\left(-\frac{Z_t}{2\pi}\iint c_1\, db_1\, d\varphi_1\right) k_{cp}+\\ &+\left(-\frac{Z_t}{2\pi}\iint f_z s_1^2 \left(\sin\chi\right)^2\, db_1\, d\varphi_1\right) k_{ns}+\\ &+\left(-\frac{Z_t}{2\pi}\iint s_1 \sin\chi\, db_1\, d\varphi_1\right) k_{np}+\\ &+\left(-\frac{Z_t}{2\pi}\iint f_z s_1^2 \sin\chi\cos\chi\sin\gamma_a\, db_1\, d\varphi_1\right) k_{cs}\end{aligned} \tag{72}$$

where we recall that

$$\begin{aligned} s_1 &= \sin\varphi_1\\ c_1 &= \cos\varphi_1\\ \chi &= \chi\left(b_1\right)\\ \gamma_a &= \gamma_a\left(b_1\right)\end{aligned} \tag{73}$$

and the double integral limits are those defined in Equation (71).

Similarly, along the feed perpendicular direction we have

$$\begin{aligned}\bar{F}_y = &\left(\frac{Z_t}{2\pi}\iint f_z s_1^2 \sin\chi\cos\gamma_a\, db_1\, d\varphi_1\right) k_{cs}+\\ &+\left(\frac{Z_t}{2\pi}\iint s_1\, db_1\, d\varphi_1\right) k_{cp}+\\ &+\left(-\frac{Z_t}{2\pi}\iint f_z s_1 c_1 \sin^2\chi\, db_1\, d\varphi_1\right) k_{ns}+\\ &+\left(-\frac{Z_t}{2\pi}\iint c_1 \sin\chi\, db_1\, d\varphi_1\right) k_{np}+\\ &+\left(-\frac{Z_t}{2\pi}\iint f_z s_1 c_1 \sin\chi\cos\chi\sin\gamma_a\, db_1\, d\varphi_1\right) k_{cs}\end{aligned} \tag{74}$$

Eventually, along the axial direction we have

$$\begin{aligned}\bar{F}_z = &\left(-\frac{Z_t}{2\pi}\iint f_z s_1 \sin^2\chi \sin\gamma_a \, db_1 \, d\varphi_1\right) k_{cs} + \\ &+ 0 \cdot k_{cp} + \\ &+ \left(\frac{Z_t}{2\pi}\iint f_z s_1 \sin\chi\cos\chi \, db_1 \, d\varphi_1\right) k_{ns} + \\ &+ \left(\frac{Z_t}{2\pi}\iint \cos\chi \, db_1 \, d\varphi_1\right) k_{np}\end{aligned} \tag{75}$$

Thanks to transformation (71) all the double integrals can be easily solved by the variable separation method, since there are no argument functions depending on both φ_1 and b_1 at the same time.

Let us now consider a face milling cutter with mechanically clamped cutting inserts, with nose radius r_ε and nominal working cutting edge angle χ_1. Let us further assume that the axial rake angle is approximately constant along the cutting edge $\gamma_a(b_1) \approx \bar{\gamma}_a$.

Along the nose radius the local working cutting edge varies according to the relation

$$\chi\left(z = a_p\right) = \arccos\left(\frac{r_\varepsilon - a_p}{r_\varepsilon}\right) \tag{76}$$

The endpoint of nose radius - where the straight part of the cutting edge begins, which is oriented according to the nominal working cutting edge angle χ_1 - is located at

$$z = a_{p\chi 1} = r_\varepsilon\left(1 - \cos\chi_1\right) \tag{77}$$

Let us first calculate the integrals along the cutting edge, by taking into account both the nose radius and the straight part of the cutting edge, as follows

$$
\begin{aligned}
I_{s\chi} &= \int_0^{B_1} \sin\chi \, db_1 = \begin{cases} (-\cos\chi_{ap} + 1)\, r_\varepsilon \text{ if } a_p < a_{p\chi 1} \\ (-\cos\chi_{ap} + 1)\, r_\varepsilon + (a_p - a_{p\chi 1}) \text{ if } a_p \geqslant a_{p\chi 1} \end{cases} \\
I_{c\chi} &= \int_0^{B_1} \cos\chi \, db_1 = \begin{cases} \sin\chi_{ap} r_\varepsilon \text{ if } a_p < a_{p\chi 1} \\ \sin\chi_1 r_\varepsilon + \cos\chi_1 \left(\frac{a_p - a_{p\chi 1}}{\sin\chi_1} \right) \text{ if } a_p \geqslant a_{p\chi 1} \end{cases} \\
I_{s2\chi} &= \int_0^{B_1} \sin^2\chi \, db_1 = \begin{cases} \frac{1}{2}\chi_{ap} r_\varepsilon - \frac{1}{4}\sin(2\chi_{ap})\, r_\varepsilon \text{ if } a_p < a_{p\chi 1} \\ \frac{1}{2}\chi_1 r_\varepsilon - \frac{1}{4}\sin(2\chi_1)\, r_\varepsilon + \sin\chi_1 (a_p - a_{p\chi 1}) \text{ if } a_p \geqslant a_{p\chi 1} \end{cases} \\
I_{sc\chi} &= \int_0^{B_1} \sin\chi\cos\chi \, db_1 = \begin{cases} \frac{1}{2}\sin^2\chi_{ap} r_\varepsilon \text{ if } a_p < a_{p\chi 1} \\ \frac{1}{2}\sin^2\chi_1 r_\varepsilon + \cos\chi_1 (a_p - a_{p\chi 1}) \text{ if } a_p \geqslant a_{p\chi 1} \end{cases}
\end{aligned}
\tag{78}
$$

Similarly, let us compute the integrals with respect to the feed motion angle φ_1

$$
\begin{aligned}
I_\varphi &= \int_{\varphi_{in}}^{\varphi_{out}} d\varphi_1 = \varphi_{out} - \varphi_{in} \\
I_{s\varphi} &= \int_{\varphi_{in}}^{\varphi_{out}} s_1 \, d\varphi_1 = -\cos\varphi_{out} + \cos\varphi_{in} \\
I_{c\varphi} &= \int_{\varphi_{in}}^{\varphi_{out}} c_1 \, d\varphi_1 = \sin\varphi_{out} - \sin\varphi_{in} \\
I_{s2\varphi} &= \int_{\varphi_{in}}^{\varphi_{out}} s_1^2 \, d\varphi_1 = \frac{1}{2}(\varphi_{out} - \varphi_{in}) - \frac{1}{4}(\sin(2\varphi_{out}) - \sin(2\varphi_{in})) \\
I_{sc\varphi} &= \int_{\varphi_{in}}^{\varphi_{out}} s_1 c_1 \, d\varphi_1 = \frac{1}{2}\left(\sin^2\varphi_{out} - \sin^2\varphi_{in}\right)
\end{aligned}
\tag{79}
$$

Accordingly, the final equation relating the average force $\bar{F}_x$ to the S&P coefficients is

$$\bar{F}_x = \underbrace{\left[-\frac{Z_t}{2\pi} f_z \left(\cos\bar{\gamma}_a I_{sc\varphi} I_{s\chi} + \sin\bar{\gamma}_a I_{s2\varphi} I_{sc\chi}\right)\right]}_{\psi_{x,cs}} k_{cs} + \underbrace{\left(-\frac{Z_t}{2\pi} I_{c\varphi} B\right)}_{\psi_{x,cp}} k_{cp} + \\ + \underbrace{\left(-\frac{Z_t}{2\pi} f_z I_{s2\varphi} I_{s2\chi}\right)}_{\psi_{x,ns}} k_{ns} + \underbrace{\left(-\frac{Z_t}{2\pi} I_{s\varphi} I_{s\chi}\right)}_{\psi_{x,np}} k_{np} \tag{80}$$

Similarly we have

$$\bar{F}_y = \underbrace{\left[\frac{Z_t}{2\pi} f_z \left(\cos\bar{\gamma}_a I_{s2\varphi} I_{s\chi} - \sin\bar{\gamma}_a I_{sc\varphi} I_{sc\chi}\right)\right]}_{\psi_{y,cs}} k_{cs} + \underbrace{\left(\frac{Z_t}{2\pi} I_{s\varphi} B\right)}_{\psi_{y,cp}} k_{cp} + \\ + \underbrace{\left(-\frac{Z_t}{2\pi} f_z I_{sc\varphi} I_{s2\chi}\right)}_{\psi_{y,ns}} k_{ns} + \underbrace{\left(-\frac{Z_t}{2\pi} I_{c\varphi} I_{s\chi}\right)}_{\psi_{y,np}} k_{np} \tag{81}$$

and

$$\bar{F}_z = \underbrace{\left(-\frac{Z_t}{2\pi} f_z \sin\bar{\gamma}_a I_{s\varphi} I_{s2\chi}\right)}_{\psi_{z,cs}} k_{cs} + \underbrace{0}_{\psi_{z,cp}} \cdot k_{cp} + \\ + \underbrace{\left(\frac{Z_t}{2\pi} f_z I_{s\varphi} I_{sc\chi}\right)}_{\psi_{z,ns}} k_{ns} + \underbrace{\left(\frac{Z_t}{2\pi} I_{\varphi} I_{c\chi}\right)}_{\psi_{z,np}} k_{np} \tag{82}$$

Finally the matrix $\mathbf{X}$ can be assembled as follows

$$\mathbf{X} = \begin{bmatrix} \psi_{x1,cs} & \psi_{x1,cp} & \psi_{x1,ns} & \psi_{x1,np} \\ \vdots & \vdots & \vdots & \vdots \\ \psi_{xN,cs} & \psi_{xN,cp} & \psi_{xN,ns} & \psi_{xN,np} \\ \psi_{y1,cs} & \psi_{y1,cp} & \psi_{y1,ns} & \psi_{y1,np} \\ \vdots & \vdots & \vdots & \vdots \\ \psi_{yN,cs} & \psi_{yN,cp} & \psi_{yN,ns} & \psi_{yN,np} \\ \psi_{z1,cs} & \psi_{z1,cp} & \psi_{z1,ns} & \psi_{z1,np} \\ \vdots & \vdots & \vdots & \vdots \\ \psi_{zN,cs} & \psi_{zN,cp} & \psi_{zN,ns} & \psi_{zN,np} \end{bmatrix} \tag{83}$$

It is worth noting that the above calculations are almost exact for the computation of the average cutting forces even when tool runout is present, or when end-mills with high axial rake angle are considered.

On the contrary, when the instantaneous cutting forces have to be estimated, in general it is not possible to apply the simplifications presented in this appendix. For example, instantaneous cutting forces at a given feed motion angle $\varphi(t)$ can be based on the integrals (78) only when the variation of cutting edge angular localization due to axial rake and depth of cut is small in comparison with cutter circumference, i.e.

$$a_p \gamma_a \ll \pi D \tag{84}$$

which is approximately true for the face milling cutters considered in this study. Nevertheless, when condition (84) is not satisfied - as in the case of helicoidal end-mills working in peripheral conditions - one has to integrate all the infinitesimal forces acting on a given flute by taking into account the variation of the feed motion angle along the engaged cutting edge, as illustrated in section 3.4.